Complex Dynamics in Systems with Many Degrees of Freedom

Thesis by
Marc S. Bourzutschky

In Partial Fulfillment of the Requirements
for the Degree of
Doctor of Philosophy

California Institute of Technology
Pasadena, California

1993

(Defended September 29, 1992)

Ein jeder lernt nur, was er kann.

J. W. von Goethe

Acknowledgements

This thesis would not have been possible without my adviser, Professor Michael Cross, whose astonishing intuition into physics always provided fresh ideas when I had reached my wits' end. At the same time, he gave me the freedom to explore whatever I wished, and rounded up financial support even in difficult economic times. I am particularly indebted to him for involving me in several teaching endeavors, which has led to some of the most rewarding moments of my stay at Caltech.

I am grateful to all the members of the Condensed Matter Physics group at Caltech for providing a friendly environment fostering both scientific and non-scientific interaction. I especially want to acknowledge many enlightening discussions with Drs. Michael Grabinski and Yuhai Tu.

My parents' encouragement has been the foundation of my educational pilgramage, and my debt to them can never be fully repaid.

Last but not least I want to thank my wife Judith, without whose loving support I would have fallen through the cracks a long time ago.

To Judith

Abstract

Complex dynamics in systems with many degrees of freedom are investigated with two classes of computational models. The models in the first class are motivated by the experimental observation of spatiotemporal chaos in strongly driven convection cells, and are designed to display chaotic evolution in discrete space and time. A local conservation law is incorporated into the equations of motion, and its importance is discussed. The central limit theorem is applied to characterize fluctuations over large uncorrelated regions, and a simple theory predicting the long wavelength properties of the models is developed and verified numerically. The applicability of the fluctuation-dissipation theorem and the maximum entropy principle to nonequilibrium systems is tested extensively. A possible application to an experimental situation is outlined.

The models in the second class are motivated by the concept of self-organized criticality, which predicts that driven dynamical systems naturally evolve to a statistically stationary state displaying scale invariance. Several scenarios of how scaling behavior can occur in dynamical systems are discussed, using ideas from dimensional analysis. A simple mean field theory for a large class of cellular automata models is developed. Extensive numerical simulations are described which test the validity of scaling forms and demonstrate possible errors resulting from finite size effects.

Contents

List of Figures

Chapter 1

Coupled Maps with Conservation Laws

Richtiges Auffassen einer Sache und
Mißverstehen der gleichen Sache
schließen einander nicht vollständig
aus.
F. Kafka

1.1 Introduction

1.1.1 Motivation

Physicists attempt to understand complex phenomena in nature by constructing model systems which shed light on essential aspects without necessarily explaining all the details. One of the most successful examples is the Navier-Stokes equation, which describes classical fluids on a macroscopic scale where microscopic degrees of freedom have been averaged out [1]. This description takes the form of a set of nonlinear partial differential equations containing only the conserved densities and 'broken symmetry' variables [2]. The underlying assumption is that fluctuations resulting from averaging over the microscopic degrees of freedom are small on the scales of interest, and can be approximated by additive Gaussian noise sources whose correlations can be determined from equilibrium statistical mechanics [3]. While this assumption has yet to be mathematically justified [4], experimental evidence overwhelmingly supports its validity, so that it appears safe to regard the Navier-Stokes equation itself as a fundamental 'microscopic' starting point of investigation. Indeed, fluctuations are often so small that they can be neglected entirely, rendering the Navier-Stokes equation purely deterministic. It should be emphasized that at this level of description the Hamiltonian nature of the underlying microscopic dynamics is no longer apparent.

Direct application of the Navier-Stokes equation itself, however, often leads to considerable mathematical difficulties when insight into cooperative dynamics on large spatial scales is desired, and further reductions in the model equations seem necessary. An example where substantial progress has been made in reducing the complexity of the problem is the classic case of Rayleigh-Bénard convection near threshold [5]. The onset of the convective instability can easily be understood from the full set of hydrodynamic equations, because nonlinear terms can be neglected. However, as the Rayleigh number of the fluid is increased, nonlinear terms are no

longer negligible and a solution to the full fluid equations is usually not possible. For weak nonlinearities, one can often obtain a reduced description for slow distortions of the linear state in terms of an *amplitude equation* [6]. While the amplitude equation is also nonlinear and in general not exactly soluble, it usually presents a considerable reduction in the complexity of the problem, for example by replacing a set of vector fields by a single scalar field. Another advantage of the amplitude equation approach is that the same equation can often be applied to seemingly different problems, allowing a unified treatment of a large variety of pattern forming systems [7].

For larger Rayleigh numbers, where nonlinear terms can no longer be treated by perturbation theory, no unifying theoretical scheme is currently available. Experimentally it is found that chaos can occur in the motion of a large number of convection rolls [8, 9]. The seminal work by Lorenz [10], which forcefully brought the possibility of chaos to the attention of physicists, was indeed intended as a model for convection in the atmosphere. By truncating a Fourier expansion of the velocity field to only two terms, Lorenz reduced the fluid equations to a set of three ordinary differential equations, which show chaos as a control parameter is increased above a certain threshold. While it is now known that the chaos in the Lorenz model is an artifact of the low order truncation of the original equations [11], the possibility of chaos in spatially extended systems has indeed been demonstrated theoretically, for example in the Kuramoto-Sivashinsky equation [12, 13].

In this chapter we discuss the effects of chaotic motion at small scales on the motion at large scales and attempt to determine whether concepts from equilibrium thermodynamics are applicable. We emphasize that the 'small scales' considered here are themselves macroscopic, i.e., we are not attempting to derive statistical mechanics from the basic Hamiltonian equations of motion. As an example for the kind of system we have in mind, we briefly describe the convection experiment by Ciliberto and Bigazzi [9, 14]. The experimental system consists of an annular cell of height 1 cm, with an inner diameter of 6 cm, and outer diameter of 8 cm. The

cell is filled with silicon oil, and a temperature gradient is applied across the height of the cell. Above the critical Rayleigh number, an almost one-dimensional chain of convection rolls appears, with their roll axes along the radius of the cell. As the temperature gradient is increased, the roll axes start oscillating about their mean position, and the interaction between adjacent rolls causes turbulent defects in the flow pattern and temperature profile. At large enough temperature gradients these defects cover the whole cell, and spatiotemporal intermittency [15] is observed. We suggest that this system can be modelled by taking as the basic unit a complete roll, or even a small set of rolls. The number of rolls ($\sim$ 30 in the experiment) is much smaller than the $\sim 10^{23}$ microscopic degrees of freedom available, but large enough so that statistical effects may come into play.

Another experimental situation which we believe may fall into this framework is the excitation of surface waves in a liquid subjected to an oscillatory driving force. It was already observed by Michael Faraday [16] that liquids placed on vertically oscillating plates develop capillary ripples at half the driving frequency. This *parametric instability* has been the subject of numerous investigations [17]. We are particularly interested in the experiments by Tufillaro et al. [18], in which it is shown that at large enough driving amplitudes the capillary ripples display spatiotemporal chaos. In these experiments, the ratio λ/L of the size of the ripples to the size of the container is $\sim 1/100$. As in the convection experiment described above, we suggest that this system may be understood by taking the basic unit to be a small domain of ripples, thereby eliminating the need to solve the full Navier-Stokes equations for the fluid.

To summarize, we attempt to model chaos in systems where the dynamics appear to be dominated by an intermediate ($\sim$ 100) number of degrees of freedom. This number, which is of course much smaller than the $\sim 10^{23}$ microscopic degrees of freedom available, is nevertheless considerably larger than the ~ 5 degrees of freedom typically studied in the context of low-dimensional chaos. Our aim is

to investigate whether statistical descriptions similar to those used in equilibrium statistical mechanics can also be used for these nonequilibrium systems.

1.1.2 Outline

The outline of this chapter is as follows: In section 1.2 we begin by using the logistic map to provide a simple introduction to chaos in systems with only one degree of freedom. We then discuss coupled maps as models for chaos in systems with many degrees of freedom, and review some of the previous work that has been done. Finally, we discuss the importance of conservation laws and introduce our own coupled map models to be studied in the remainder of the chapter.

In section 1.3 we describe numerical experiments that characterize the chaotic state, with particular emphasis on the Lyapunov spectrum. We also discuss the importance of the correlation length, and speculate on the existence of a well defined infinite volume limit in our coupled map models.

In section 1.4 we derive a Langevin equation which correctly predicts the long wavelength limit of the dynamic structure factor of our coupled map models. We also comment on the importance of nonlinear terms in the Langevin equation.

In section 1.5 we study the response of our coupled map models to a small external field, motivated by the idea that a fluctuation-dissipation theorem may hold even for nonequilibrium systems. We then explain why a fluctuation-dissipation theorem will not apply in general.

In section 1.6 we discuss several numerical experiments that test the applicability of thermodynamic ideas based on the idea of maximizing an entropy.

In section 1.7 we comment on a recent experiment, where an attempt was made at a thermodynamic analysis of a chaotic system.

Finally, we summarize our results in section 1.8.

1.2 Coupled Map Models

1.2.1 The Logistic Map

Much of our knowledge about chaotic dynamical systems has been gained from the study of discrete iterated maps. These maps obey equations of motion of the form:

$$\mathbf{y}^{n+1} = \mathbf{f}(\mathbf{y}^n), \qquad n = 0, 1, 2, \ldots \tag{1.1}$$

where n is a discrete time index, and $\mathbf{y} \in R^m$. The simplest case occurs when $\mathbf{y}$ is a simple scalar [19], and we will use the famous *logistic map* to give an elementary introduction to chaos. The logistic map is defined by:

$$y^{n+1} = 4ay^n(1 - y^n), \qquad n = 0, 1, 2, \ldots \tag{1.2}$$

where $0 < y^0 < 1$ and $0 < a < 1$. This map has a long history as a simple nonlinear model of population dynamics [20]. The sequence $\{y^i,\ i = 0, 1, 2, \ldots\}$ can display a variety of patterns; we will describe some of them which introduce some of the concepts and terminology used in the remainder of this chapter.

The simplest pattern displayed by Eq. (1.2) is the appearance of a fixed point, where y^i approaches a constant independent of i. In addition to the trivial fixed point $y^i = 0$, we can find all the other fixed points y by setting $y^{n+1} = y^n \equiv y$:

$$y = 1 - 1/4a. \tag{1.3}$$

The stability of any given fixed point can be determined by evaluating the local slope $s = (dy^{n+1}/dy^n)$. For the trivial fixed point $y = 0$ we have $s = 4a$, while all the other fixed points have $s = 2 - 4a$. This slope gives an effective growth rate of

an infinitesimal perturbation δx^0:

$$\delta x^n = e^{n\lambda}\delta x^0, \tag{1.4}$$

$$\lambda = \log(|s|). \tag{1.5}$$

Evidently, fixed points will be stable under small perturbations if $\lambda < 0$. For non-zero fixed points stability requires $a < 3/4$, while the trivial fixed point $y = 0$ is stable for $a < 1/4$.

As a is increased beyond $3/4$, the fixed points become unstable and first give way to periodic orbits with period two. For still larger a, these orbits become unstable to orbits of period four. This trend of period-doubling continues; for large n, orbits with period 2^n occur for:

$$a \approx a_\infty - \frac{A}{\delta^n}, \tag{1.6}$$

where A is a constant. This famous result is due to Feigenbaum, who showed that $\delta \approx 4.66920\ldots$ is a universal constant, occurring quite generally for maps that have a quadratic maximum [21]. At first sight it might seem reasonable to call the behavior of the logistic map at the accumulation point $a = a_\infty \approx 0.892\ldots$ 'chaotic', since no stable orbits with finite period exist. However, a strict definition of chaos involves sensitive dependence on initial conditions, as we will discuss below, and it turns out that the logistic map at the accumulation point does not satisfy that criterion. Nevertheless, *period-doubling cascades* are one possible route to chaos, and for $a > a_\infty$ the logistic map indeed shows chaotic behavior for several ranges of a, albeit interrupted by windows of periodic motion. The periodic doubling route to chaos has been observed in many experiments in such diverse areas as hydrodynamics [22], optics [23], acoustics [24], and biology [25].

As noted above, a strict definition of chaos involves sensitivity to initial condition, meaning that nearby points in phase space should separate exponentially fast with time. The divergence of phase space trajectories is characterized by *Lyapunov*

exponents [26], and the appearance of positive Lyapunov exponents is an unambiguous sign of chaos. As an example, we now describe the logistic map Eq. (1.2) for $a = 1$, where an exact solution is possible [27]. It is easy to check by direct substitution that for $a = 1$ Eq. (1.2) is solved by:

$$y^n = \sin^2(2^n \pi \beta), \tag{1.7}$$

for arbitrary initial conditions parametrized by β, $0 < \beta < 1$. Periodic orbits correspond to rational values for β, and are always unstable. If we represent β in binary notation as $0.\beta_1\beta_2\ldots$, we see that on each iteration all the digits of β are shifted one position to the left (due to the multiplication by two), and then the digit in front of the decimal point is lost (due to the periodicity of the sine function). It is now evident that two different initial conditions, corresponding to different values of β, will separate exponentially with the Lyapunov exponent $\lambda = \log(2)$, corresponding to one binary digit per iteration. When no exact solution is available, the Lyapunov exponent of an iterated map is evaluated as:

$$\lambda = \lim_{n\to\infty} \frac{1}{n} \sum_{i=1}^{n} \log \left| \frac{df(y^i)}{dy} \right|. \tag{1.8}$$

The existence of this limit is ensured if ergodicity holds, i.e., if time averages can be replaced by averages over an *invariant probability measure* ρ. For iterated maps, ρ must satisfy:

$$\rho(f^{-1}(x)) = \rho(x). \tag{1.9}$$

In the case of the logistic map Eq. (1.2) with $a = 1$, one finds:

$$\rho(x) = \frac{1}{\pi} \frac{1}{\sqrt{x(1-x)}}. \tag{1.10}$$

This measure provides another way to calculate the Lyapunov exponent:

$$\lambda = \int_0^1 dx \frac{\log|4-8x|}{\pi\sqrt{x(1-x)}} = \log(2). \tag{1.11}$$

The probability measure ρ will in general not be unique. However, as apparently first conjectured by Kolmogorov [28], the inevitable presence of noise in any physical system may lead to a unique *physical measure.*

To summarize, chaos can be conveniently characterized by positive Lyapunov exponents, which describe the exponential divergence of trajectories in phase space. In most physical systems, we expect chaotic systems to be ergodic, with a unique physical measure. The Lyapunov spectrum is then independent of initial conditions and of the coordinate system chosen, and can be evaluated by a time average. As is the case of statistical mechanics, ergodicity will usually be difficult to prove rigorously.

1.2.2 Many Degrees of Freedom

We now turn to the case where $\mathbf{y}$ in Eq. (1.1) is a vector, rather than a scalar as in the logistic map. Even when $\mathbf{y}$ has only two components, some qualitatively new behavior compared to the simple scalar case can occur. For example, one can construct *area preserving* maps [29], which have properties very similar to Hamiltonian systems. This is possible because one of the components of $\mathbf{y}$ can play the role of a 'momentum'.

The most important new feature of concern to us, however, is that instead of only one Lyapunov exponent, one now obtains a whole spectrum of exponents. In general, in systems with m degrees of freedom, there will be m exponents. These exponents show, roughly speaking, how trajectories diverge in different orthogonal directions in phase space.

To define the Lyapunov spectrum, consider the case where $\mathbf{y}$ in Eq. (1.1) has m

components, and denote the i-th component at time n by y_i^n, $i = 1, 2, \ldots, m$. At any given time n, the linearized behavior of the map is then characterized by the $m \times m$ Jacobian matrix $\mathbf{J}^n$:

$$[\mathbf{J}^n]_{ij} = \frac{\partial f_i(\mathbf{y}^n)}{\partial y_j}. \tag{1.12}$$

We now define the matrix $\mathbf{T}^n$ by the product:

$$\mathbf{T}^n = \mathbf{J}^{n-1}\mathbf{J}^{n-2}\ldots\mathbf{J}^0, \tag{1.13}$$

and determine the m eigenvalues Λ_i of the positive definite matrix $\mathbf{T}^n(\mathbf{T}^n)^t$. The Lyapunov exponents λ_i are then given as:

$$\lambda_i = \lim_{n\to\infty} \frac{1}{2n} \log(\Lambda_i). \tag{1.14}$$

The *multiplicative ergodic theorem* due to Oseledec [30] guarantees the existence of the exponents, independent of initial conditions, in the case where there exists an ergodic measure. We should emphasize that this is a highly nontrivial result, since the matrices $\mathbf{J}^i$ will usually not commute. Indeed, no direct formula is presently known for evaluating the Lyapunov exponents for $m > 1$, even if the underlying probability measure is known [26].

If the Lyapunov exponents are sorted in decreasing order, $\lambda_1 \geq \lambda_2 \geq \cdots \geq \lambda_m$, the sum of the first k exponents can be interpreted as the growth rate of a k-volume element averaged over the phase space trajectory of the map [26]. Because of the complicated stretching and contraction associated with positive and negative Lyapunov exponents, it is generally believed that in the infinite time limit, the motion of a system having both positive and negative exponents takes place on a fractal object called a *strange attractor*. Fractal objects are characterized by non-integer dimensions [31], and several conjectures have been put forth to relate the Lyapunov exponents to various topological and information theoretical dimensions [26], but few rigorous results have been established.

We now review some specific iterated multi-dimensional maps, which have been used to study chaos in spatially extended systems. An obvious way to introduce spatial dependence into Eq. (1.1) is to simply interpret the vector **y** as representing a one-dimensional lattice, where the component y_i corresponds to the lattice position i. Such systems are referred to as *coupled map lattices*, and their study was pioneered by Kaneko [32]. He introduced the following particular model, which has since been studied in a variety of contexts:

$$y_i^{n+1} = f(y_i^n) + \frac{\epsilon}{2}\{f(y_{i+1}^n) - 2f(y_i^n) + f(y_{i-1}^n)\}, \tag{1.15}$$

where the notation is as in Eq. (1.1), except that i is now a discrete lattice index, $1 \leq i \leq L$, where L is the system size. The map function $f(x)$ is usually chosen to be either the logistic map or the circle map $f(x) = x + A\sin(2\pi x) + D$. The coupling strength ϵ is typically varied between 0 and 1.

We now summarize briefly some of the work that has been done using Eq. (1.15). Kaneko's original work consisted primarily of a classification of the behavior as a function of the coupling strength ϵ and the nonlinear parameter in the local map function $f(x)$, e.g., 'a' if $f(x)$ is the logistic map. He found a variety of different phenomena, ranging from the formation of complex patterns, to the correlated motion of defects [32].

Several groups [33, 34, 35] have used coupled map lattices to study the phenomenon of spatiotemporal intermittency [15]. An interesting conjecture by Pomeau [36], proposing to describe intermittent transitions in terms of directed percolation, has also led to various investigations of nonequilibrium phase transitions using coupled map lattices [37].

Bunimovich and Sinai [38] have shown that for weak coupling and certain conditions on the map function $f(x)$, a mapping to a 2D statistical mechanics spin model is possible, where the discrete time index plays the role of the second dimension.

Several other interesting and ambitious questions have been addressed using

coupled map models, with results that still need to be considered as rather speculative. For example, Crutchfield and Kaneko [39] have constructed a coupled map model similar to Eq. (1.15), which displayed chaotic motion over a transient time which increased exponentially with the system size. The authors then argue that many complex phenomena in nature, including turbulence, may really be transients where the asymptotic state is never observed. Another interesting suggestion, based on numerical investigations of coupled map models, is that chaos is a purely local phenomenon [40, 41], i.e., spatially coarse-grained variables will not be chaotic.

Finally, there is an interesting neural network model consisting of infinitely many sites [42], where every lattice site couples to all the other sites. The dynamics in this case can be reduced to a self-consistent equation for a single site, allowing an exact determination of the largest Lyapunov exponent. The model shows a sharp transition from stationary to chaotic behavior as the nonlinear map parameter is tuned, and represents one of the few model systems with many degrees of freedom where exact results with chaotic behavior have been obtained.

1.2.3 Conservation Laws

We constructed our own coupled map model based on Eq. (1.15), but we also incorporate a conservation law [43]. There are a number of important reasons for imposing conservation laws.

Firstly, conservation laws occur naturally in many situations we might try to describe. For example, in the Rayleigh-Bénard convection experiment described in the introduction, the average fluid density is conserved. Similarly, in the surface wave experiments we described, the average level of fluid in the container is conserved. Indeed, in the derivation of the Navier-Stokes equation conservation laws play the central role, since mass, momentum, and energy conservation persist through coarse graining procedures.

Secondly, apparent conservation laws can arise through broken symmetries. An

example is the superfluid velocity in a Bose condensed system $\mathbf{v}_s \propto \nabla\phi$ with ϕ the phase of the macroscopic wavefunction: the dynamics of $\mathbf{v}_s$ is governed by a conservation law, deriving in fact from the equation for ϕ that describes the broken gauge symmetry:

$$\begin{aligned} \partial_t \phi &= F\{\nabla\phi, \ldots\} \\ \text{so that} \quad \partial_t \mathbf{v}_s &= \nabla F\{\mathbf{v}_s, \ldots\}, \end{aligned} \tag{1.16}$$

which has the form of a conservation law. Here F cannot depend on ϕ itself by the basic phase symmetry. An analogous case in nonequilibrium systems is the Kuramoto-Sivashinsky equation [12]:

$$\partial_t u(x,t) = -\partial_x^2 u - \partial_x^4 u - u\partial_x u. \tag{1.17}$$

This equation may be derived as the dynamics of a phase variable ϕ which here characterizes displacements of a periodic pattern (broken translational symmetry) with $u = \partial_x \phi$.

Finally, it is known that in equilibrium systems interesting long length scale dynamics usually derives from conservation laws: in the absence of these, long wavelength properties often reduce to simple averages over independent, rapidly fluctuating microscopic regions, usually yielding uninteresting results. We expect the same to be true for dissipative systems, although there may still be interesting questions on how to characterize the short length scale behavior in systems without conserved quantities.

With these considerations, we modify Eq. (1.15) to the following model which satisfies a discrete version of the continuity equation:

$$y_i^{n+1} = y_i^n + g(y_{i+1}^n, y_i^n) - g(y_i^n, y_{i-1}^n). \tag{1.18}$$

The role of the current term in the continuity equation is played by the scalar function g. For simplicity, we impose $g(x,y) = -g(y,x)$ to make the model invariant under the parity transformation $i \leftrightarrow -i$. We enforce periodic boundary conditions:

$$y^n_{i+L} = y^n_i. \tag{1.19}$$

The conserved 'mass' Q is evidently given by:

$$Q = \sum_{i=1}^{L} y^n_i. \tag{1.20}$$

We consider two different choices for g, which we will refer to as 'model A' and 'model B'. Model A is defined by:

$$\begin{aligned} g(x,y) &= f(x) - f(y), \\ \text{where} \quad f(x) &= ax + bz(1-z) \\ \text{with} \quad z &\equiv |x| \pmod 1, \end{aligned} \tag{1.21}$$

where a and b are constants. The functional form of f is shown in Fig. 1-1.

Model B is defined by:

$$\begin{aligned} g(x,y) &= \frac{2f(x-y)}{1+x^2+y^2}, \\ \text{with} \quad f(x) &= ax + b\sin(cx), \end{aligned} \tag{1.22}$$

where a, b, and c are constants.

The change from Eq. (1.15) to Eq. (1.18) introduces some slight complications for the choice of map function. For example, in the non-conserved model Eq. (1.15) it is easy to ensure that the lattice amplitudes are always bounded: if $f(x)$ and ϵ range between 0 and 1, the lattice amplitudes are also bounded between 0 and 1. In the conserved model Eq. (1.18) this is no longer the case, and the map function has to be

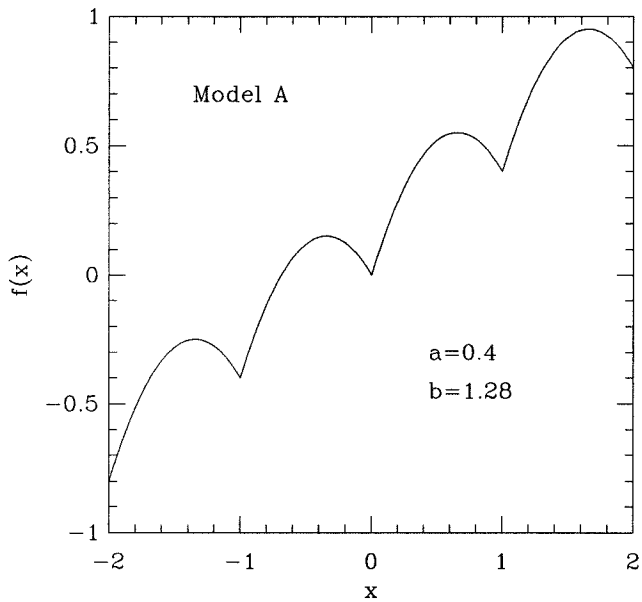

Figure 1-1: Map function for model A.

chosen appropriately not only to ensure the boundedness of the lattice amplitudes, but also to avoid the approach of a trivial fixed point or periodic orbit. Model A and model B will remain bounded if the diffusion constant a satisfies $0 < a < 1/2$. Avoiding trivial periodic orbits is not as easily arranged. We have found empirically that the most likely periodic orbit is a 'zig-zag' state where adjacent lattice sites have amplitudes z_1 and z_2 which are exchanged every iteration, leading to a state of period two. The linear stability of this state can easily be determined from the equations of motion, and the map parameters can then be chosen to make this orbit unstable. For more complicated periodic orbits a direct stability analysis is not practical, and we rely on trial and error and the methods described in the next section to ensure chaotic motion.

1.3 Characterization of Spatially Extended Chaos

1.3.1 Lyapunov Exponents

We now describe simple numerical experiments that have shed some light on the nature of the extended chaotic state and which motivated the search for a simple long wavelength description.

For $b = 0$, model A (cf. Eq. (1.21)) evidently reduces to a finite difference approximation to the one-dimensional linear diffusion equation. Almost all initial configurations decay to a spatially uniform state $y_i^n = \text{const}$. As we increase b, we observe oscillations of period two, and at larger b oscillations of period four. At a critical value b_c we measure a positive Lyapunov exponent, signaling the onset of chaos. The onset of chaos is in the form of 'local defect turbulence', i.e., most of the lattice sites are still oscillating with period four and only a small number of sites shows chaotic behavior. In Figure 1-2 we show how the largest Lyapunov exponent λ_{max} depends on the nonlinear control parameter b. We find that just above the onset of chaos, $\lambda_{max} \sim (b - b_c)^{1/2}$.

It is tempting to regard λ_{max} as a kind of order parameter (or rather disorder parameter) [44], which is zero below the onset of chaos. Indeed, for the logistic map Eq. (1.2) it has been shown that the envelope of the curve $\lambda(a)$ has the scaling form $\lambda(a) \sim (a - a_c)^{\tau}$, with a universal constant $\tau \approx 0.4498\ldots$ [45]. We should emphasize, however, that the scaling relations seen in the logistic map are a result of the period-doubling cascade. This is quite different from the scaling relations observed in second order phase transitions, which occur only in the thermodynamic limit of infinite volume.

We are mainly interested in the situation well above the onset of chaos, where a whole set of positive Lyapunov exponents appears. We therefore not only require the largest exponent, but the full Lyapunov spectrum. Considerable care is required to obtain accurate numerical results and we detail our computational procedure in

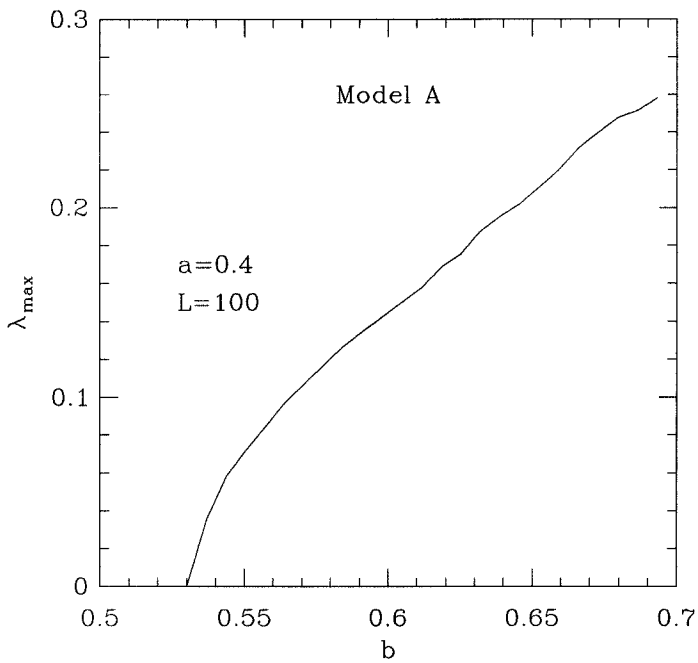

Figure 1-2: Maximum Lyapunov exponents.

the Appendix.

In Figure 1-3 we show the Lyapunov spectra for two different lattice sizes. These spectra show several interesting features.

One obvious feature is that the sum of the Lyapunov exponents is greater than zero. For a set of N autonomous ordinary first order differential equations of the form:

$$\frac{d\mathbf{x}_i}{dt} = \mathbf{f}_i(\mathbf{x}_1, \ldots, \mathbf{x}_N), \qquad i = 1, 2, \ldots, N \tag{1.23}$$

it is easily shown that the sum of the Lyapunov exponents gives the average expansion of a volume element:

$$\sum_{i=1}^{N} \lambda_i = \langle \nabla \cdot \mathbf{f} \rangle, \tag{1.24}$$

where $\langle \ldots \rangle$ denotes time averaging. This in particular leads to the usual definition of a dissipative system as one in which the phase space volume contracts on average, i.e., the sum in Eq. (1.24) is negative. For discrete maps there does not exist a

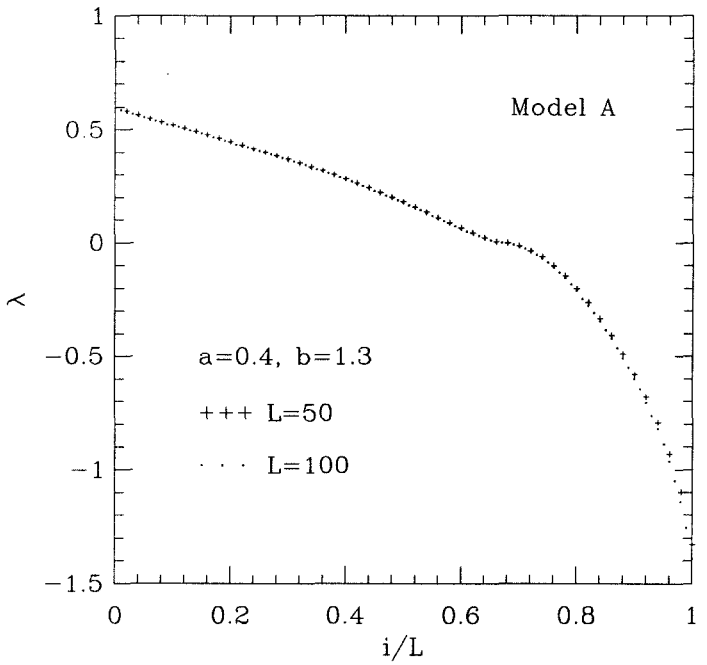

Figure 1-3: Lyapunov spectra.

continuous trajectory in phase space, and Eq. (1.24) does not apply. Nevertheless, it remains an interesting question how to characterize the effective dimension of the chaotic attractor. In general, fractal objects must be characterized by a whole family of *generalized dimensions* [46]. We mention only the *information dimension* D_I, since a relation between D_I and the Lyapunov exponents has been conjectured [47]. To obtain D_I, we divide phase space into N small boxes with linear dimension ϵ, and determine the probability p_i that the dynamical system is found in box i. Then

$$D_I = \lim_{\epsilon \to 0} \lim_{N \to \infty} \frac{\sum_{i=1}^{N} p_i \log(p_i)}{\log(\epsilon)} = \lim_{\epsilon \to 0} -\frac{S(\epsilon)}{\log(\epsilon)}, \tag{1.25}$$

where $S(\epsilon)$ can be interpreted as the 'information content' of the partition [48]. The Lyapunov dimension D_L is defined as:

$$D_L = j + \frac{\sum_{i=1}^{j} \lambda_i}{|\lambda_{j+1}|}, \tag{1.26}$$

where j is the largest integer such that:

$$\sum_{i=1}^{j} \lambda_i \geq 0. \tag{1.27}$$

It can be rigorously shown that $D_I \leq D_L$ [49], and it was suggested that in fact an equality holds [47]. Counterexamples to this conjecture are known [50, 26], and we must evidently consider our coupled map model as yet another one. This is somewhat unfortunate, since numerical dimension estimates are only feasible for low-dimensional systems ($d \sim 5$), because the numerical complexity increases exponentially with d [51]. As described in the Appendix, the numerical complexity of Lyapunov spectra is $\sim d^3$, allowing calculations with much larger d. However, it is not yet clear how useful the knowledge of one or more generalized dimensions is when the number of degrees of freedom is as large as in the coupled map models, and we do not address this issue further in this work.

Another interesting feature of the Lyapunov spectrum (cf. Figure 1-3) is an approximate point of inflection near $\lambda = 0$. Some mathematical arguments for singularities in the density of Lyapunov exponents exist for certain models of intermittent turbulence [52], but there is no clear connection of those arguments to the situation here. Obviously, one exponent is always trivially zero because of the conservation law (i.e., a vector for which all components are equal does not change under the dynamics and is thus always an eigenvector with eigenvalue one), but perhaps a connection can be established between small but non-zero exponents and the slow modes of the system. A point of inflection also appears in the spectrum of model B, indicating that it might be quite generic. An obvious possibility is that the negative exponents are simply due to the diffusive modes. This is most easily seen by solving the linearized equations, for example model A with $b = 0$, for which we can find the Lyapunov exponents analytically:

$$\lambda_k = \log(|1 - 4a \sin^2(\pi k)|), \tag{1.28}$$

where k ranges from 0 to the zone boundary $k = 0.5$ in steps of the reciprocal lattice vector $1/L$. For $k \ll 1$ we then obtain:

$$\lambda_k \approx -4a\pi^2 k^2, \tag{1.29}$$

clearly showing parabolic behavior.

In the strongly nonlinear chaotic regime, the notion of Fourier analysis is at first sight not useful, because it is essentially based on the principle of linear superposition. For example, as pointed out by Eckmann and Ruelle [26], the experimental observation of a continuous power spectrum can either indicate that the system explores an infinite number of dimensions in phase space, or that the system evolves nonlinearly on a finite-dimensional attractor. Nevertheless, it may happen that some of the degrees of freedom can be separated out and subjected to a traditional Fourier analysis. In our coupled map models, a trivial example is the Fourier mode with zero wavevector, which is not affected by the nonlinear dynamics due to the conservation law. We can attempt a similar analysis by numerically measuring the temporal decay of the spatial Fourier transform of the space-time correlation function for finite wavevectors, as discussed in section 1.4 below. We indeed find that Fourier modes with wave vector k decay exponentially in time, with time constants $\tau_k \sim k^2$. However, the magnitudes of the τ_k do not agree with the inverse of the Lyapunov exponents of Figure 1-3, suggesting that further work using a different approach is necessary.

Perhaps the most interesting feature of Figure 1-3 is that the exponents for two different system sizes lie on top of one another, if their coordinates are rescaled by the system size. This implies that the fraction of exponents which lie in a given range does not change with the system size. For example, the mean rate of information production, called the *Kolmogorov-Sinai entropy* [26], is believed to be given by the sum of the positive Lyapunov exponents. In Figure 1-3 this quantity is then clearly additive. The existence of additive quantities hints at the possibility of a

thermodynamic formalism; we will explore this question further in section 1.6 below. Another implication of additive quantities is simply that the system size is much larger than a certain correlation length, such that averaging over the system amounts to averaging over many uncorrelated regions. We can then apply the central limit theorem to these averages and predict Gaussian distributions, as discussed in the next section.

1.3.2 Correlation Lengths

To investigate whether our coupled map models indeed have short range correlations, we can measure the equal time correlation function $S(r)$ [3, 53]:

$$S(r) = \left\langle (y_i^n - \langle y \rangle)(y_{i+r}^n - \langle y \rangle) \right\rangle , \tag{1.30}$$

where $\langle \ldots \rangle$ denotes averaging over both i and n. Before presenting our results, we list a few caveats that need to be observed in interpreting correlation functions.

In many cases corresponding to short range correlations, we expect $S(r) \sim \exp(-r/\xi)$ for large r, defining the correlation length ξ. However, the actual form of $S(r)$ may be considerably more complicated. For example, unless one length scale completely dominates all the others (as happens near second order phase transitions), there is no reason to even expect $S(r)$ to take on the form $f(r/\xi)$ with a uniquely defined ξ. In addition, $S(r)$ may display complex oscillations about zero as a function of r, not simply describable as 'antiferromagnetic'. We therefore believe that a reasonable definition of 'short range correlations' needs to be quite flexible, perhaps in terms of the distance over which correlations can be distinguished from experimental noise. In this context, we also emphasize that algebraic decays in correlation functions are not necessarily an indication of long range correlations, as is often supposed. The power laws observed near second order phase transitions are the result of, and not the cause of, a diverging correlation length. For example, a

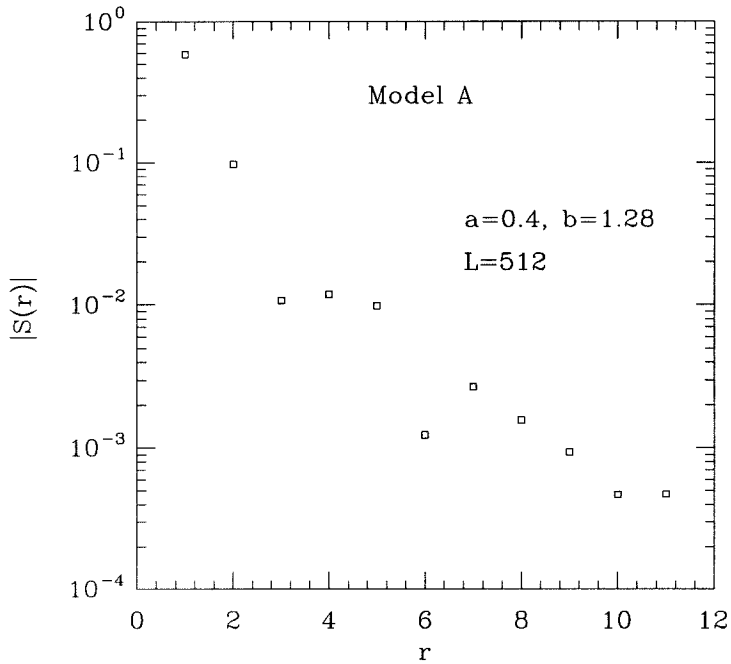

Figure 1-4: Spatial correlation function $|S(r)|$.

correlation function which decays as $(r/\xi)^{-3}$, where ξ is a *microscopic* length, can very well reflect short range correlations. One might object that in this case higher order moments will diverge, but it must be remembered that correlation functions are statistically averaged quantities, and that higher order moments may need to be averaged over a different distribution, because experimental noise sources are not necessarily independent.

We now return to our coupled map models, and show $|S(r)|$ for model A in Figure 1-4. While $|S(r)|$ does not have a simple exponential form, it decays rapidly, indicating a finite correlation length of approximately two lattice spacings.

Appealing to the central limit theorem, we now expect that fluctuations of spatially averaged quantities will have a Gaussian distribution, since the average will be over many uncorrelated regions. This will be true even if the decay of correlations is algebraic rather than exponential, provided the relevant power is large enough.

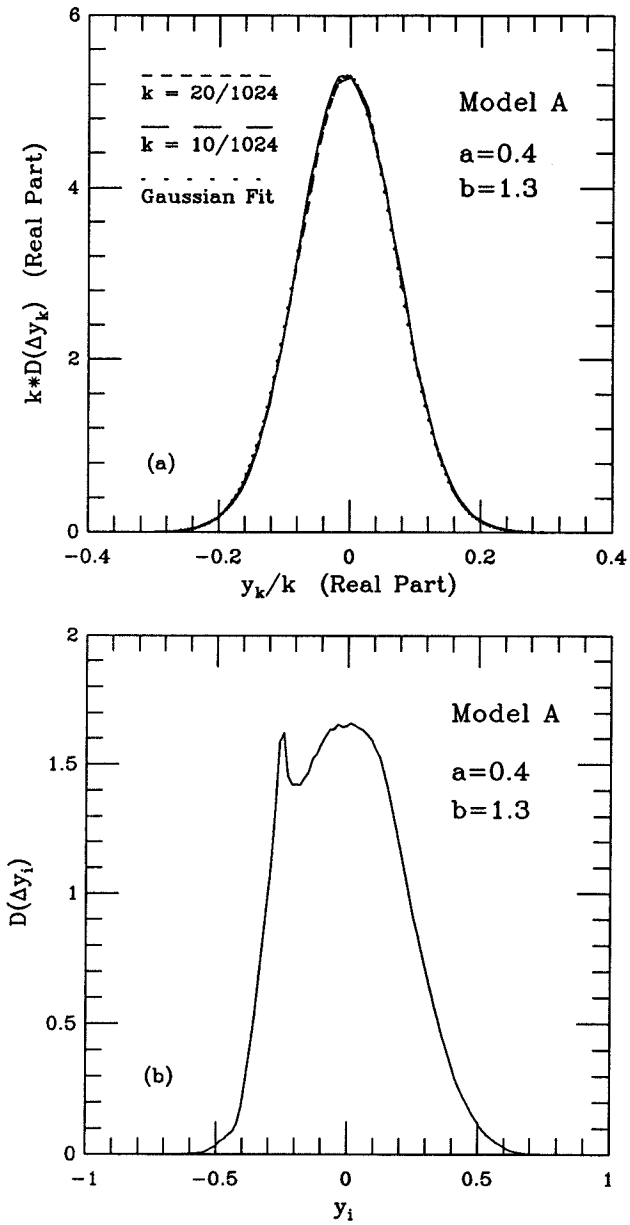

Figure 1-5: Distribution of (a) Fourier amplitudes, (b) Lattice amplitudes.

As a simple example, we consider the spatial Fourier transform of the lattice amplitudes:

$$y_k^n = \frac{1}{\sqrt{L}} \sum_{j=1}^{L} e^{2\pi i j k} y_j^n, \tag{1.31}$$

where k is a multiple of the reciprocal lattice vector $1/L$. From the central limit theorem, we now expect the fluctuations of y_k^n to have a Gaussian distribution, even for short wavevectors. The only requirement is of course that the system size L is large enough. Since y_k^n is complex, we have computed both the real and imaginary parts of the fluctuations of the Fourier amplitudes $\Delta y_k^n = y_k^n - \langle y_k^n \rangle$, averaged over n. In Figure 1-5a, we show the distribution $D(\Delta y_k)$ of the real part of y_k^n, together with a Gaussian fit, which evidently describes the distribution well. The imaginary part of Δy_k^n also has a Gaussian distribution, with the same variance. We have also computed the distribution of $\Delta S_k^n = |\Delta y_k^n|^2$, finding an exponential distribution as expected from the sum of the squares of two independent Gaussian distributed variables. $D(\Delta y_k)$ should be contrasted with the distribution $D(\Delta y_i)$ of fluctuations of a single lattice amplitude, shown in Figure 1-5b. The latter distribution is of course strongly affected by the choice of map function, and cannot be expected to have a simple form. It is not even symmetric about $y = 0$, since the equations of motion Eq. (1.21) do not have that symmetry.

Also note that the width of $D(\Delta y_k)$ scales with wave vector. This is related to the vanishing of the structure factor $S(k)$ as $k \to 0$ in this model, which we will discuss further in section 1.4.

1.4 Structure Factor and Langevin Equation

In section 1.3.2 we saw that Fourier modes display Gaussian fluctuations. This suggests that it may be possible to construct stochastic model equations which contain simple Gaussian distributed noise terms, and which can reproduce some of the behavior of the maps. A general ansatz for such stochastic equations is the

Langevin equation [55, 56]:

$$\frac{\partial y_i}{\partial t} = F_i(y) + \eta_i(t), \tag{1.32}$$

where y is a random field, and F is in general a nonlinear functional of y. The label i may be discrete or continuous. η is a stochastic noise term, which is delta correlated in time and independent of y. Without loss of generality, we can assume $\langle \eta \rangle = 0$. If we furthermore assume a Gaussian distribution for η, all the moments of η are completely specified by the second moment:

$$\langle \eta_i(t)\eta_j(t') \rangle = 2D_{ij}\delta(t - t'), \tag{1.33}$$

where D_{ij} is a symmetric positive definite diffusion matrix [56]. We emphasize that Eq. (1.32) is a *stochastic* differential equation for the *stochastic* process y, and the solution will consist of the moments $\langle y(t) \rangle$, $\langle y^2(t) \rangle$, etc., averaged over a suitable ensemble. Instead of Eq. (1.32) it is also possible to derive a master equation for the probability distribution $P(y,t)$ [57]. This results in a Fokker-Planck equation for P from which the moments of y can be computed, giving equivalent results to the Langevin approach.

To apply these general results to our coupled map models, we need to derive the form of F in Eq. (1.32). For the moment, we will assume that all nonlinear terms can be neglected. Since we are interested in the long wavelength behavior, we assume in addition that we can coarse grain the discrete lattice and time indices to obtain partial differential equations, rather than finite difference equations. Finally, we assume that we can expand the spatial dependence in a power series of the wavevector k. The lowest power of k that can occur in the expansion is k^2, because the constant term is absent due to the conservation law, and the term linear in k violates the parity symmetry $k \leftrightarrow -k$. In addition, we also need to expand the noise term η. In principle, the lowest power of k allowed is now k, but as we shall see more directly below, that term is absent. This can also be deduced from Figure 1-

5a, where it is seen that the width of the Gaussian distribution of the fluctuations scales with the wavevector, introducing an additional factor of k.

We can now write down the resulting Langevin equation:

$$\frac{\partial y(k,t)}{\partial t} = -k^2(Dy(k,t) + \eta(k,t)), \tag{1.34}$$

where D is a diffusion constant and the noise term η has correlations of the form:

$$\langle \eta(k,t)\eta(k',t)\rangle = A\delta(k+k')\delta(t-t'), \tag{1.35}$$

where A is an effective noise amplitude.

To give a more transparent but less general derivation, we start directly with the definition of the spatial Fourier transform Eq. (1.31):

$$y_k^{n+1} = \frac{1}{\sqrt{L}} \sum_{j=1}^{L} e^{2\pi ijk} y_j^{n+1}. \tag{1.36}$$

We now substitute for y_j^{n+1} using the equations of motion for model A, Eq. (1.18) and Eq. (1.21):

$$\begin{aligned} y_k^{n+1} &= \frac{1}{\sqrt{L}} \sum_{j=1}^{L} e^{2\pi ijk} \{ y_j^n + f(y_{j-1}^n) - 2f(y_j^n) + f(y_{j+1}^n) \} \\ &= y_k^n - \frac{4\sin^2(\pi k)}{\sqrt{L}} \sum_{j=1}^{L} e^{2\pi ijk} f(y_j^n), \end{aligned} \tag{1.37}$$

where we have made use of the periodic boundary conditions. In the long wavelength limit, we can approximate $y_k^{n+1} - y_k^n$ by $\partial_t y$, and $\sin^2(\pi k)$ by $\pi^2 k^2$. If we set $f(y_j^n) \sim cy_j^n + \eta$, we directly arrive at Eq. (1.34). The Langevin equation is therefore basically the original equation, with all nonlinear terms replaced by random noise, which also leads to a renormalized diffusion constant. In real space, it is a simple linear diffusion

equation:

$$\partial_t y = D\partial_x^2 y + \partial_x^2 \eta, \tag{1.38}$$

where the noise correlation takes the form:

$$\langle \eta(x,t)\eta(x',t')\rangle = A\delta(x-x')\delta(t-t'). \tag{1.39}$$

We now investigate whether nonlinear terms are important in our Langevin equation. Naively, one would expect their effect to be small at long wavelengths, since the noise averages to small values there. In recent years, Langevin models similar to Eq. (1.38) have been studied intensively because of the possibility that nonlinear terms can in fact lead to non-integral powers of k in the correlation function and long time tails in the dynamics through the buildup of the noise at long wavelengths. A famous example is the random-force driven Burgers equation [58], which has been studied in many contexts, in particular that of the behavior of stochastically driven interfaces [59]. In the present case, simple arguments show that no relevant nonlinear terms are expected to appear in Eq. (1.38). As an example, we add to Eq. (1.38) the nonlinear term $\lambda\partial_x^2 y^2$ which is the simplest term satisfying both the conservation law and parity symmetry. To study the effect at long wavelengths, we use the method of 'power counting' [3] as applied in the context of renormalization group theory.

We perform a scaling transformation $x \to bx$, $t \to b^z t$, and $y \to b^\chi y$, where z and χ are scaling exponents to be determined. Including the nonlinear term, Eq. (1.38) then becomes:

$$\partial_t y = Db^{z-2}\partial_x^2 y + \lambda b^{\chi+z-2}\partial_x^2 y^2 + b^{z/2-\chi-5/2}\partial_x^2 \eta, \tag{1.40}$$

where we have used Eq. (1.39) to determine the scaling of the noise term. For $\lambda = 0$, scale invariance is evidently achieved for $z_0 = 2$ and $\chi_0 = -3/2$. When $\lambda \neq 0$, a simple scaling solution is no longer possible. Power counting consists of simply looking

at the effective scaling of the nonlinear term, which is $b^{\chi_0+z_0-2} = b^{-3/2}$ in our case. As b is increased, i.e., the length scale considered gets larger, the effective strength of the nonlinear term decreases, therefore becoming irrelevant in the renormalization group sense. The power counting argument can be made rigorous by constructing a perturbation expansion for the nonlinear term, and showing that the perturbation becomes irrelevant in the limit of small wavevectors [3]. It is easy to check that all other analytic nonlinear terms consistent with the symmetries one might add to Eq. (1.38) are similarly irrelevant. Relevant nonlinearities will therefore only be expected to appear if the conservation law or the parity symmetry is broken. This is the case with the random-driven Burgers equation, which has the form:

$$\partial_t y + y\partial_x y = D\partial_x^2 y + \partial_x \eta, \tag{1.41}$$

where the noise correlation is as in Eq. (1.39). Power counting now shows that the nonlinear term scales as $b^{1/2}$, and is therefore relevant at large length scales. Eq. (1.41) has been analyzed by Forster, Nelson, and Stephen [58] using dynamic renormalization group theory.

Returning to the linear Langevin equation Eq. (1.38), we can now make several predictions. The most important quantity we can compute from the Langevin equation is the space-time correlation function:

$$S(r,t) = \langle (y(r'+r,t'+t) - \langle y \rangle)(y(r',t') - \langle y \rangle) \rangle \tag{1.42}$$

where averaging is over r' and t'. The Fourier transform of $S(r,t)$ is the *dynamic structure factor* $S(k,w)$:

$$S(k,\omega) = \int_{-\infty}^{\infty} dk \int_{-\infty}^{\infty} d\omega \, e^{-i(kx-\omega t)} S(r,t). \tag{1.43}$$

The Wiener-Khinchin theorm [55] shows that $S(k,\omega) = \langle |y(k,\omega)|^2 \rangle$. Using this

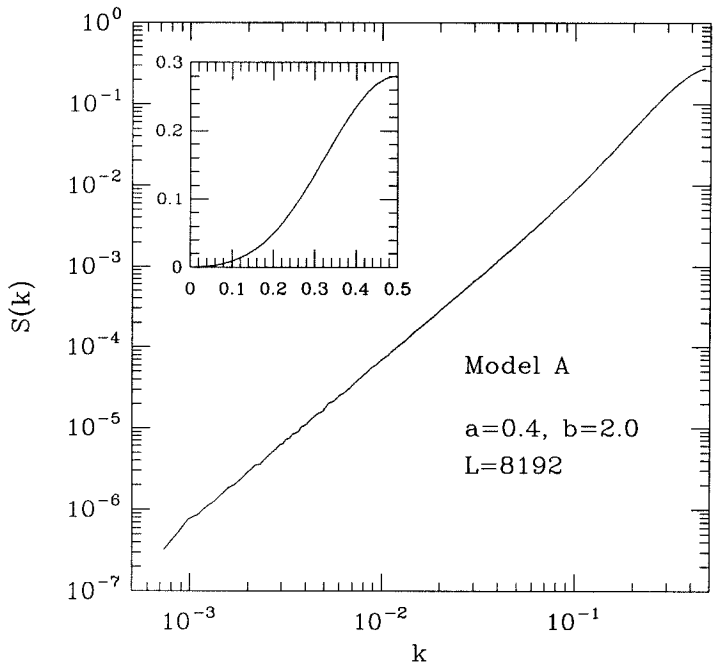

Figure 1-6: Static structure factor.

relation in Eq. (1.38), we find directly:

$$S(k,\omega) = \frac{ADk^4}{(Dk^2)^2 + \omega^2}. \tag{1.44}$$

As shown in Figure 1-6 and Figure 1-7, we find numerical results consistent with:

$$S(k,t) = S(k)e^{-Dk^2 t}, \tag{1.45}$$

$$S(k) = Ak^2. \tag{1.46}$$

Performing Fourier transforms in time, these results agree with Eq. (1.44). We also find that the effective diffusion constant D is somewhat larger than the diffusion constant expected from the linearized equation.

The vanishing of the static structure factor $S(k)$ as $k \to 0$ for model A is related to the absence of a term linear in k in front of the noise term. This is due to

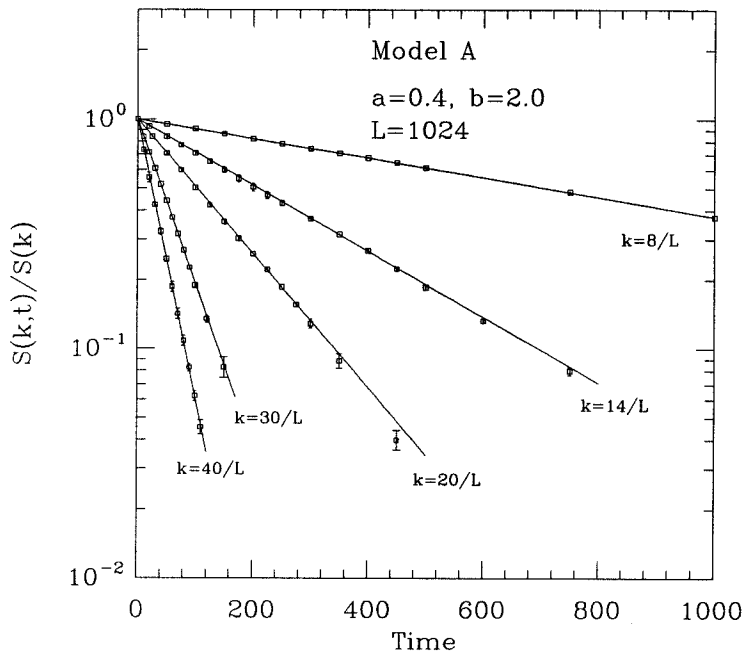

Figure 1-7: Dynamic structure factor.

the particular form of model A, and is not a result of parity symmetry. Indeed, performing the same analysis leading to Eq. (1.37) on model B, we find that the expected Langevin equation now takes the form:

$$\partial_t y = D\partial_x^2 y + \partial_x \eta, \tag{1.47}$$

with the correlation of η still given by Eq. (1.39). The structure factor for model B will therefore have a factor of k^2 missing compared to model A. A numerical computation of $S(k)$ for model B (cf. Figure 1-8) indeed shows that $S(k) \to$ const. as $k \to 0$.

To summarize, we have derived a Langevin equation for our coupled map models, which can correctly predict the long wavelength form of the dynamic structure factor. We have shown that the conservation law and parity symmetry of the system are sufficient to exclude nonlinear terms from the long wavelength description. As far as

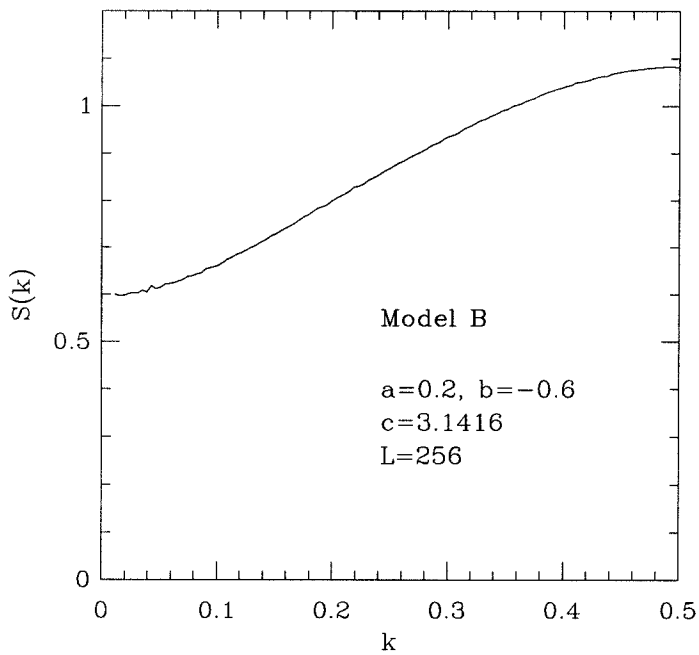

Figure 1-8: Static structure factor for model B.

two point correlation functions are concerned, we have been able to replace a very complicated nonlinear deterministic system by a simple stochastic one. A similar analysis has been carried out by Zaleski [60], who showed numerically that at long wavelengths the deterministic Kuramoto-Sivashinski equation Eq. (1.17) has two point correlation functions like the random-driven Burgers equation Eq. (1.41).

1.5 Linear Response and Fluctuation-Dissipation Theorem

In the previous section, we derived a Langevin equation which contained a Gaussian noise term. In thermodynamic applications, this noise typically has a thermal origin, and this provides us with additional information. A famous example is the case of Brownian motion of a single particle in one dimension in a fluid at temperature T

[55]. The Langevin equation for this system takes the form:

$$\frac{dv}{dt} + \gamma v(t) = \eta(t), \tag{1.48}$$

where the mass of the particle has been scaled to unity, γ is a damping constant, and η is a Gaussian random force due to the fluid, which has zero mean and a second moment given by:

$$\langle \eta(t)\eta(t') \rangle = \Gamma \delta(t - t'), \tag{1.49}$$

where Γ is at this stage undetermined. Performing ensemble averaging we immediately obtain:

$$\langle v(t)^2 \rangle = v_o^2 e^{-2\gamma t} + \frac{\Gamma}{2\gamma}(1 - e^{-2\gamma t}), \tag{1.50}$$

where v_0 is the initial velocity. At large times, the particle will be in equilibrium with the fluid, and $\langle v(\infty)^2 \rangle = k_B T$, where k_B is Boltzmann's constant. We thus obtain for the noise amplitude:

$$\Gamma = 2\gamma k_B T. \tag{1.51}$$

This equation is a simple example of the *fluctuation-dissipation theorem* [61].

The general fluctuation-dissipation theorem (FDT) is a relation between equilibrium correlation functions and linear response functions. In Fourier space, we can define the linear response function $\chi(k, \omega)$ by the relation:

$$\langle y(k, \omega) \rangle = \chi(k, \omega) h(k, \omega), \tag{1.52}$$

where h is a small field applied to y. The FDT for near equilibrium thermodynamic systems provides a relation between the temperature T, the dynamic structure factor $S(k, \omega)$, and the susceptibility $\chi(k, \omega)$:

$$T = \frac{\omega S(k, \omega)}{2 \operatorname{Im}(\chi(k, \omega))}. \tag{1.53}$$

In near equilibrium systems this relation is true for all k and ω. Using the dispersion relation [2]

$$\chi(k,\omega=0) = P\int_{-\infty}^{\infty} \frac{d\omega}{\pi} \frac{\mathrm{Im}(\chi(k,\omega))}{\omega}, \tag{1.54}$$

where P denotes the principal value, we can integrate Eq. (1.53) over ω and relate T to the static structure factor and static response functions:

$$T = \frac{S(k,t=0)}{\chi(k,\omega=0)}. \tag{1.55}$$

The FDT relation Eq. (1.53) was originally derived for Hamiltonian equilibrium systems, but several authors have suggested generalizations to more complicated situations. A particularly interesting idea is due to Leith [62], who proposed to apply the FDT to climate prediction. For example, knowledge of the natural fluctuations in the atmosphere would be sufficient to predict the climatic response to a small increase in carbon dioxide concentration, with the help of the FDT. However, the relations derived by Leith are only exact for a system of harmonic oscillators. In addition, determining the covariance matrix of climate fluctuations to sufficient accuracy to usefully apply the FDT may be a difficult problem [63].

In another attempt at generalizing the FDT, Hohenberg and Shraiman [53] have suggested that one might be able to use the FDT to define a useful 'temperature' even for nonequilibrium systems, by simply using the right hand side of Eq. (1.53), perhaps in the limit $k \to 0$ and $\omega \to 0$. If this limit exists and indeed defines an effective 'temperature' T_e even for nonequilibrium systems, there may be several useful applications. For example, T_e might provide constraints on the effective noise term in the Langevin equation. Another useful application for T_e would be the analog of a thermometer: If two coupled systems have the same value of T_e, they should be in equilibrium, i.e., there should be no net flow of the conserved quantity between them.

Accordingly, we study the response of a coupled map lattice to a small applied

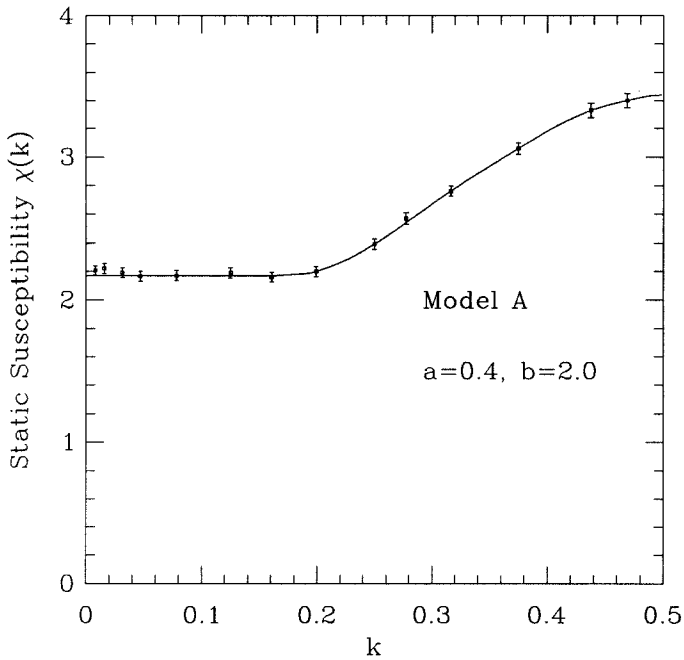

Figure 1-9: Static susceptibility.

field, chosen so as to preserve the conservation law and reflection symmetry of the map. The equation of motion Eq. (1.18) is thus modified to:

$$y_i^{n+1} = y_i^n + g(y_{i+1}^n, y_i^n) - g(y_i^n, y_{i-1}^n) + h_{i+1}^n - 2h_i^n + h_{i-1}^n, \tag{1.56}$$

where we concentrate on static fields $h_j^n = h\cos(2\pi jk)$ with fixed wavenumber k. The static susceptibility χ_k is then:

$$\chi_k = \lim_{h\to 0} \frac{2\langle y_k^n \rangle}{h}, \tag{1.57}$$

where averaging is over n. Numerical calculations of χ_k for model A and model B are shown in Figure 1-9 and Figure 1-10 respectively. At long wavelengths, we find χ_k to be essentially independent of k.

This result can easily be understood in terms of the Langevin equation by includ-

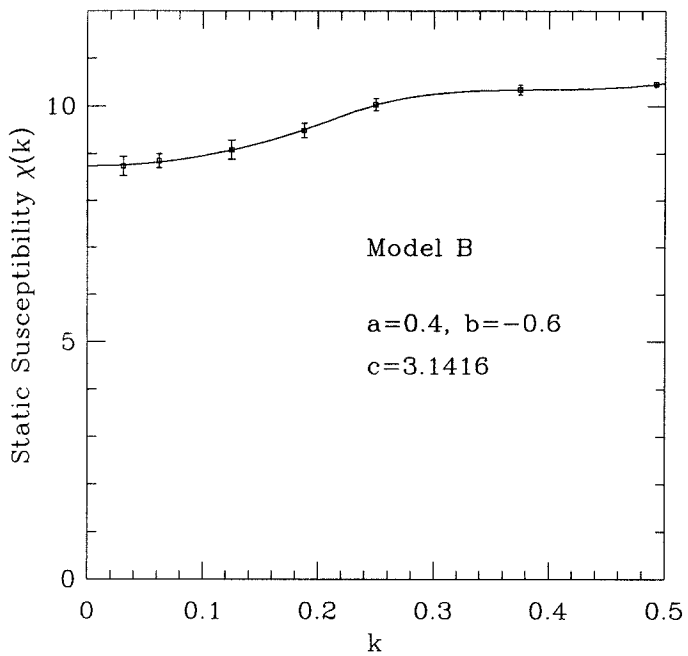

Figure 1-10: Static susceptibility for model B.

ing an additional term $\partial_x^2 h$ on the right hand side of Eq. (1.38). Since the applied field h should be uncorrelated with the effective internal noise η, one immediately finds that $\chi(k) = 1/D$. We have checked the consistency of this result by comparing the values of D obtained from $\chi(k)$ and $S(k,\omega)$ for model A (cf. Figures 1-9 and 1-7). We find numerically that $D = 0.45 \pm 0.02$ from $\chi(k)$ and $D = 0.470 \pm 0.008$ from $S(k,\omega)$, showing good agreement.

Returning to the fluctuation-dissipation ratio Eq. (1.55), we now deduce for model A that $T_e \sim k^2$. In the long wavelength limit, this effective temperature always vanishes, indicating that T_e does not have the desired properties. At the simplest level, the k^2 dependence of the effective temperature in model A comes from the extra gradient in the noise term of Eq. (1.38) as compared with the conventional ansatz for diffusional Langevin equations. However, the breakdown of the constant ratio between response and correlations can be traced to a more general flaw in the

formulation, namely our lack of knowledge of how the applied field couples to the probability functional of the system. For Hamiltonian systems, the applied fields are known to appear in the thermodynamic equations together with their conjugate fields; e.g., a magnetic field $\mathcal{H}$ appears in the internal energy through a relation of the form $\mathcal{H}dM$, where M is the magnetization. We therefore also know the form of the probability distribution $e^{-\beta\mathcal{H}}$. For nonequilibrium systems, we do not have a corresponding formalism.

A simple example may be useful here to illustrate the problem. Consider the long wavelength description of the dynamics of a single conserved variable in an equilibrium system. Following Hohenberg and Halperin [3], the thermodynamics may be defined through the entropy S and its density s:

$$S = S_0 + \int \{s'\delta q(x) + \frac{1}{2}K[\delta q(x)]^2 - h(x)\delta q(x)\} d^d x, \tag{1.58}$$

where $s' = (\partial s/\partial q)|_{q=q_0}$, and $K = (\partial^2 s/\partial q^2)|_{q=q_0}$ (which plays the role of an elastic constant) and we have expanded in small fluctuations $\delta q = q - q_0$ about a uniform equilibrium value q_0. For conserving dynamics, one obtains from Eq. (1.58) the equation of motion:

$$\begin{aligned} \dot{\delta q} &= \gamma\nabla^2(\frac{\delta S}{\delta q}) + \nabla\eta(x,t) \\ &= \gamma K\nabla^2\delta q + \nabla\eta(x,t) - \gamma\nabla^2 h(x,t), \end{aligned} \tag{1.59}$$

where γ is a kinetic coefficient, and η is a Gaussian stochastic noise term with strength F:

$$\langle\eta(x,t)\eta(x',t')\rangle = F\delta(x-x')\delta(t-t'). \tag{1.60}$$

For an applied field $h(x,t) = h_{k\omega}e^{ikx-i\omega t}$ the average response $\delta q = \delta q_{k\omega}e^{ikx-i\omega t}$

calculated from Eq. (1.59) yields a susceptibility:

$$\begin{aligned} \chi(k,w) &= \frac{\delta q_{k\omega}}{h_{k\omega}} \\ &= \frac{\gamma k^2}{-i\omega + \gamma K k^2}. \end{aligned} \tag{1.61}$$

Similarly, one obtains the dynamic structure factor:

$$\begin{aligned} S(k,w) &= \langle (\delta q_{k\omega})^2 \rangle \\ &= \frac{k^2 F}{\omega^2 + (\gamma K k^2)^2}, \end{aligned} \tag{1.62}$$

and consequently the static structure factor:

$$S(k) = \langle (\delta q_k)^2 \rangle = \frac{F}{\gamma K}. \tag{1.63}$$

However, averaging over the probability distribution $e^{-F/T}$ shows that

$$\langle (\delta q_k)^2 \rangle = 2T/K \tag{1.64}$$

so that the noise strength is related to the thermodynamic temperature via

$$F = 2\gamma T. \tag{1.65}$$

Using Eqs. (1.61), (1.62), and (1.65), the dynamic fluctuation-dissipation theorem Eq. (1.53) is immediately verified in the long wavelength limit.

Let us now repeat this analysis in the way we are forced to for a nonequilibrium system. Instead of defining the coupling to an external field through Eq. (1.58), we need to introduce a field $\bar{h}$ into the dynamics; and we do not know the division of the diffusion constant D into stiffness and kinetic parameters:

$$\dot{\delta q} = D\nabla^2 \delta q + \nabla \eta(x,t) - \nabla^2 \bar{h}(x,t). \tag{1.66}$$

From this we obtain:

$$\begin{aligned} \bar{\chi}(k,\omega) &= \frac{\delta q_{k\omega}}{\bar{h}_{k\omega}} = \frac{k^2}{-i\omega + Dk^2} \\ S(k,\omega) &= \frac{k^2 F}{\omega^2 + (Dk^2)^2} \end{aligned} \tag{1.67}$$

so that for the proposed definition of an effective temperature

$$T_e = \frac{\omega S(k,\omega)}{2\,\mathrm{Im}(\bar{\chi}(k,\omega))} \tag{1.68}$$

we find $T_e = F/2$.

Comparing with Eq. (1.39) for the equilibrium system we obtain:

$$T_e = \gamma T \tag{1.69}$$

depending on the kinetic coefficient γ. Without further knowledge about γ and its k and ω dependence, T_e cannot be expected to measure T. These are exactly the results found for our coupled map systems.

Although in the case of model B, $S(k)$ and $\chi(k)$ both approach a constant as $k \to 0$, so that $S(k)/\chi(k) \to$ constant, we would not expect this value to have the same importance as in equilibrium systems. It is also clear comparing Figure 1-8 and Figure 1-10 that $S(k)/\chi(k)$ is k dependent for large k.

1.6 Thermodynamics

1.6.1 Postulates of Thermodynamics

In section 1.5 we have seen that the fluctuation-dissipation theorem is not directly applicable to nonequilibrium systems. We therefore turn to an alternative point of view, which only depends on the concept of *thermodynamic equilibrium*, rather than

on small fluctuations about equilibrium.

Thermodynamics can be formulated as a series of basic postulates which are independent of the presumably underlying concepts of statistical mechanics. Indeed, the foundation of statistical mechanics is still a subject of intense investigation [65], while thermodynamics is logically complete. There are alternative ways of formulating the postulates of thermodynamics, and we will follow very closely the presentation by Callen [64], with comments on how the postulates may relate to our coupled map models.

Postulate I *There exist equilibrium states of simple systems that, macroscopically, are characterized completely by the internal energy U, the volume V, and the mole numbers $N_1, N_2, \cdots, N_r$ of the chemical components.*

We can hypothesize that our coupled maps are 'simple systems', whose macroscopic states are completely characterized by the conserved quantity Q, and the number of lattice sites N. A 'simple system' in this context means that the model system is isotropic and translationally invariant, as we have ensured with the basic equations of motion of the coupled map lattices. To experimentally determine and characterize the equilibrium state is of course a major challenge, and below we will describe several computer experiments with this goal in mind.

Postulate II *There exists a function (called the entropy S) of the extensive parameters of any composite system, defined for all equilibrium states and having the following property. The values assumed by the extensive parameters in the absence of an internal constraint are those that maximize the entropy over the manifold of constrained equilibrium states.*

The question of the existence of an entropy function that is maximized is the main motivation for our investigations. Consider, for example, two different coupled map lattices whose conserved quantities are Q_1 and Q_2 respectively. Suppose that

the two maps are allowed to interact in such a way that Q can flow from one map to the other, with the constraint that $Q_1 + Q_2 =$ remains constant. Then maximizing the entropy will select a *particular* Q_1' and Q_2'. One difficulty of course is how to implement the interaction. The interaction has to impose no constraints of its own, so that the dynamics can sample all possible states consistent with the conservation law in order to find the particular state with maximum entropy. As we shall see, ensuring this in a computational model can be quite difficult. Another more obvious requirement is that the entropy of the 'interaction' be small compared to the entropies of the two systems, to ensure the additivity required in the following postulate:

Postulate III *The entropy of a composite system is additive over the constituent subsystems. The entropy is a continuous and differentiable function of the energy.*

Using these postulates, it is now possible to introduce the concept of temperature. Consider again two systems whose equilibrium states are characterized by the conserved quantities Q_1 and Q_2. The total entropy S of the two systems is, by additivity, simply the the sum of the entropies of the two systems: $S = S_1(Q_1) + S_2(Q_2)$. Maximizing S with the constraint that $Q_1 + Q_2 = Q$ is constant immediately gives the result that at equilibrium:

$$\frac{dS_1}{dQ_1} = \frac{dS_2}{dQ_2} \equiv \frac{1}{T}, \tag{1.70}$$

defining the temperature T.

1.6.2 Heat Bath Algorithms

In this section we describe some numerical experiments which test the postulates described in section 1.6.1. One of the consequences of the existence of a temperature is the transitivity of thermal equilibrium: If X is in equilibrium with Y, and Y is in equilibrium with Z, then X is in equilibrium with Z. We test this transitivity by

using three different coupled maps X, Y, and Z, obtained from model A by different choices of the nonlinear control parameter b (cf. Eq. (1.21)). The lattice sizes L_X, L_Y, and L_Z are chosen such that $L_Z = L_Y \ll L_X$. We implement coupling between two lattices by modifying the equation of motion Eq. (1.18) at the endpoints of the lattices to contain a current term linear in the difference of the lattice amplitudes in the two lattices. For example, if X and Y are coupled, the equation of motion for the endpoint of X becomes:

$$y_X^{n+1}(L_X) = y_X^n(L_X) - g_X(y_X^n(L_X),\, y_X^n(L_X - 1)) + d(y_Y^n(1) - y_X^n(L_X)), \qquad (1.71)$$

where different lattices are distinguished by subscripts, and the lattice positions are given in brackets. We arrange the two lattices on a ring, so that we obtain analogous equations to Eq. (1.71) for $y_X(1)$, $y_Y(1)$, and $y_Y(L_Y)$. The coupling strength is parametrized by d.

Starting with a random initial configuration with total $Q = 0$, we in turn couple Y and Z to X and iterate the new equations of motion until steady state is achieved. The steady state is characterized by new values of the conserved quantities Q_Y and Q_Z in Y and Z, while the change in the mean value of Q_X should be small because of the large lattice size L_X.

In Figures 1-11 a, b, and c we illustrate the sequence of events described above by plotting the time evolution of Q for three situations: The thermalization of two small lattices Y and Z with a large lattice X is shown in Figures 1-11a and 1-11b; in Figure 1-11c we test for equilibrium of Y and Z when initialized with the values of Q generated from the equilibration with X. For convenience, we normalize Q by the system size and denote the result by q, e.g., $q_X = Q_X/L_X$.

The transitivity of equilibrium appears to hold very well, with the small shifts in q_Y and q_Z actually seen being qualitatively consistent with those expected due to the finite size of X. In Figure 1-11d we show the time average of the local lattice amplitudes for maps X and Z, accumulated after steady state had been reached.

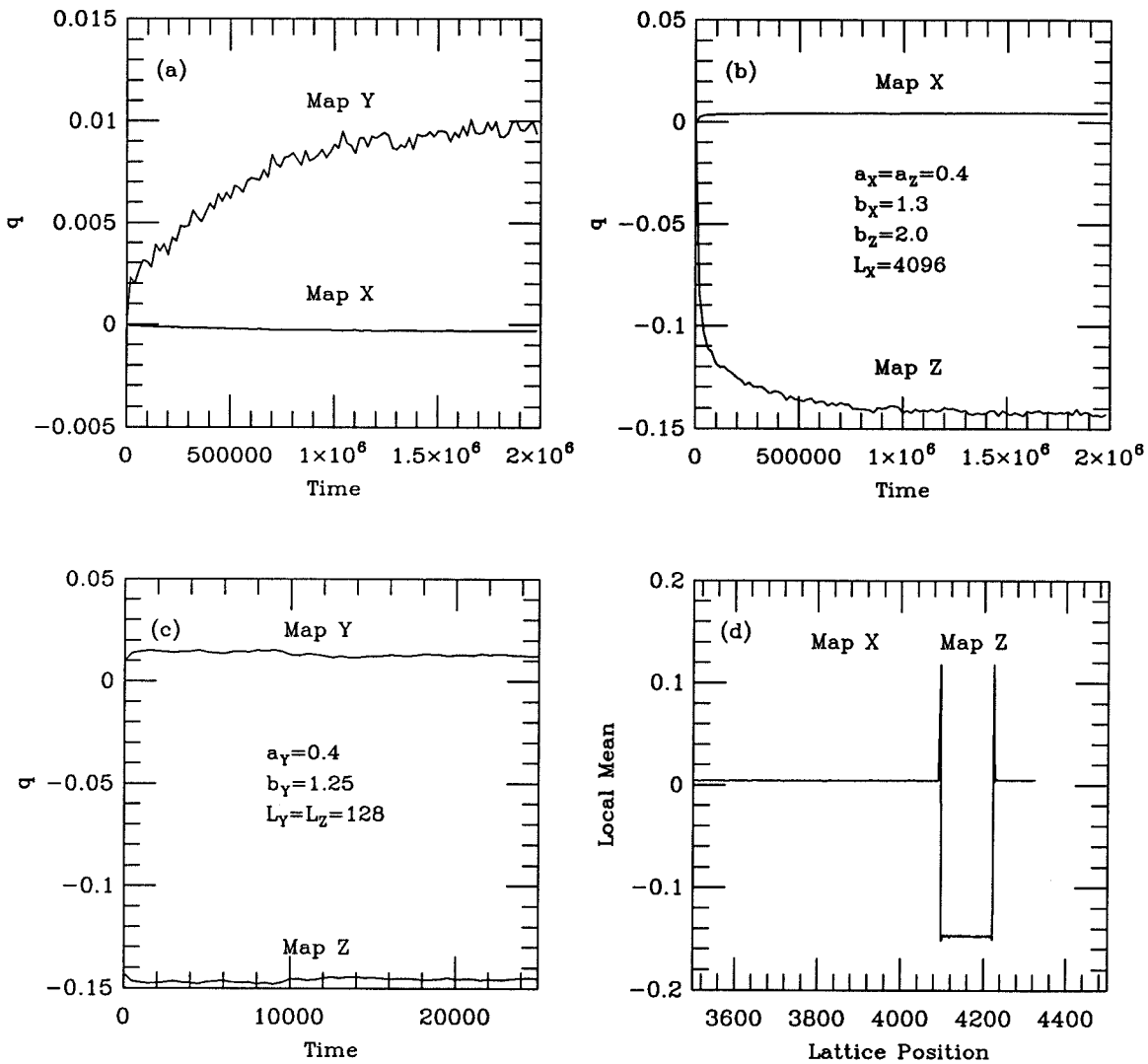

Figure 1-11: Time evolution of q (a) Y coupled to X (b) Z coupled to X (c) Y coupled to Z. (d) Time average of local means.

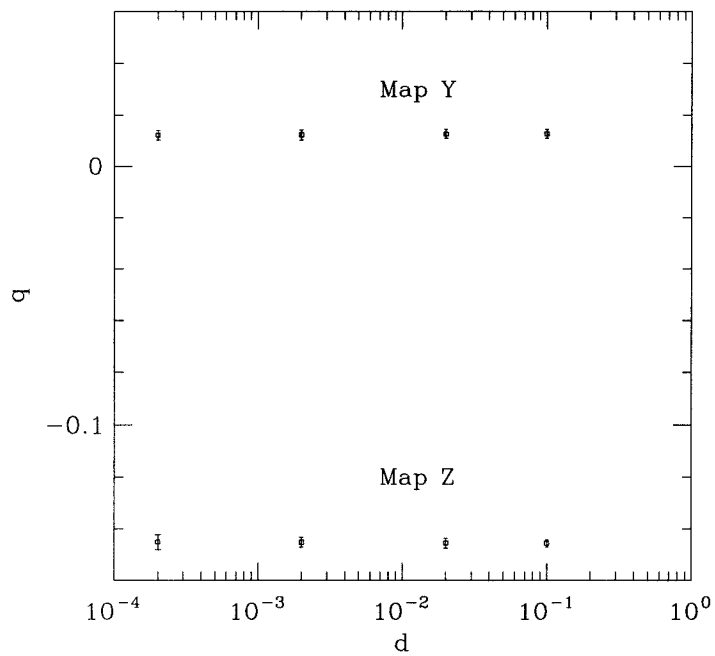

Figure 1-12: q as a function of coupling strength d.

Except very close to the interface, the local means are constant throughout each lattice, supporting the idea that each lattice has reached local equilibrium.

We also test whether the equilibrium values of q reached are independent of the coupling strength d. In Figure 1-12 we show the equilibrium values of q_Y and q_Z as a function of d; no significant dependence is found for $d < 0.1$.

In addition to the coupling strength d, it is also important to check different functional forms of the coupling. We therefore replace Eq. (1.71) by:

$$\begin{aligned} y_X^{n+1}(L_X) &= y_X^n(L_X) - g_X(y_X^n(L_X), y_X^n(L_X - 1)) \\ &\quad + d\tanh(\alpha(y_Y^n(1) - y_X^n(L_X))), \end{aligned} \tag{1.72}$$

where the parameter α parametrizes the nonlinearity of the coupling function. If there indeed exists a thermodynamic limit, then for large system sizes L and small coupling strengths d, the equilibrium values of q should be independent of α. In our

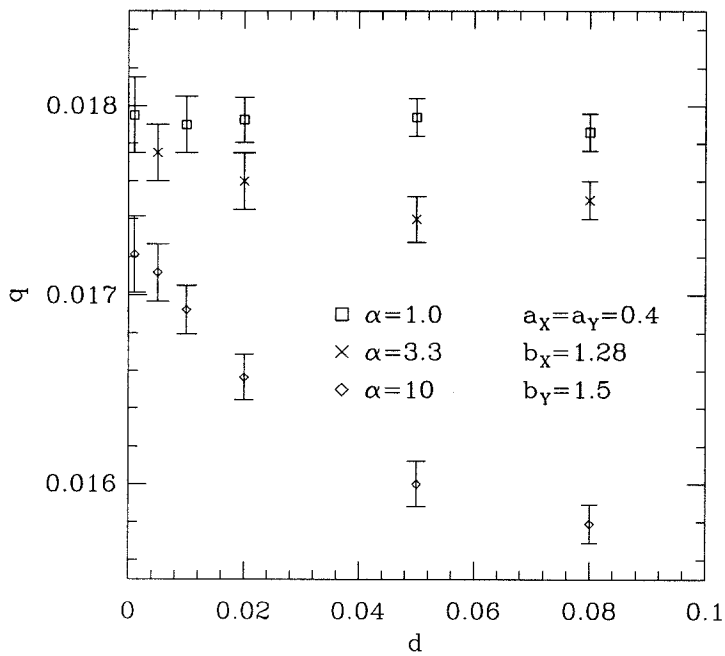

Figure 1-13: q as a function of coupling function.

numerical experiments, we choose two coupled maps X and Y with equal length L, and with an initial $q = 0$. For a fixed α and d we then determine the equilibrium value of q as a function of system size. We extrapolate the results to infinite system size (the convergence goes roughly as $1/L$) and plot the extrapolated values of q as a function of d and α in Figure 1-13. The error bars are rather large due to the uncertainties in the extrapolations, but the results seem to converge to a unique limit.

An alternative test for thermodynamic equilibrium consists of coupling three maps arranged on a ring, and monitoring the current flowing around the loop. If the three maps reach equilibrium, there should be no net current flow. In our numerical simulations, we do find persistent currents, but they are small compared to the shifts of the means between two lattices, as is evident in Figure 1-14, where we show a typical time average of the local means. The persistent currents are barely

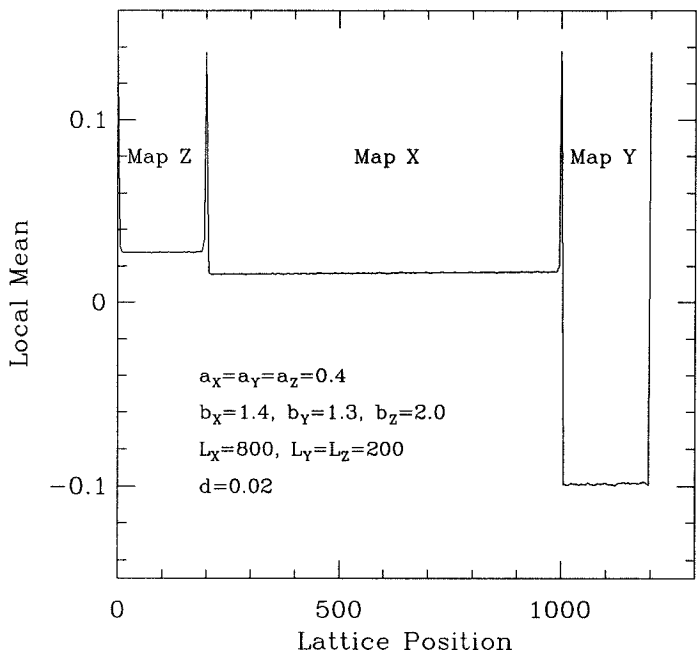

Figure 1-14: Persistent currents in three maps on a ring.

discernible as a non-zero slope of the profile of the means across each lattice. We find numerically that the magnitude of the persistent currents scales roughly as d/L, where L is the system size and d is the coupling strength. A current scaling as $1/L$ leads to a constant offset in q, and would question the thermodynamic equilibrium picture, but our numerical resolution does not allow any firm conclusions.

Assuming that the thermodynamic picture does hold, we can test it further by checking whether the distribution of q between the three maps is consistent with that found in the temperature bath experiments where two maps are coupled at a time. To do this, we increase the size L_X of one of the three lattices, and determine the corresponding rearrangement of q. The infinite system limit is approached approximately as $(1/L_X)^{1/2}$ (cf. Figure 1-15). Within error bars, the extrapolated means agree with those obtained from the heat bath experiments described previously.

While the numerical experiments described strongly suggest that thermodynamic

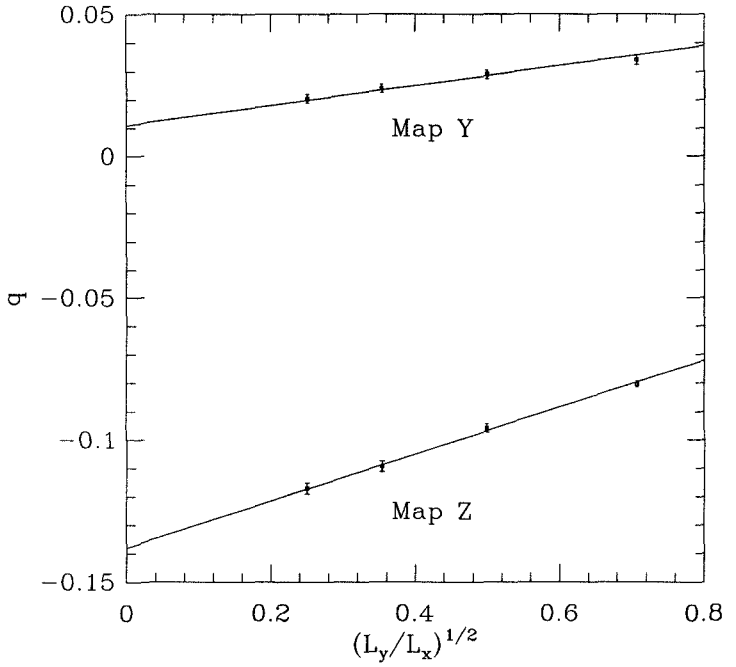

Figure 1-15: Dependence of q_Y and q_Z on L_X.

considerations may be applicable to the coupled map models considered here, the straightforward application of 'standard' thermodynamic ideas is difficult. As an example of these difficulties, we attempt to apply the *Einstein fluctuation theorem* [66]: If there exists an entropy function S which depends only on the conserved quantity Q, then small fluctuations of Q about its equilibrium value should have a Gaussian distribution of width $\partial^2 S/\partial Q^2$. Measuring the fluctuations as a function of Q should then provide an indirect way to measure the entropy. Now, if S and Q are extensive quantities, it follows that the mean square fluctuations should scale as $1/L$. However, for model A we find that the fluctuations instead scale as $1/L^2$. This is shown in Figure 1-16, where we plot the mean square fluctuations of Q in map X, while coupled to map Y, as a function of the system size $L_X = L_Y \equiv L$.

This result can be traced to the k^2 behavior of the structure factor $S(k)$ at long wavelengths (cf. Figure 1-6). To show this, consider the mean square value σ_N

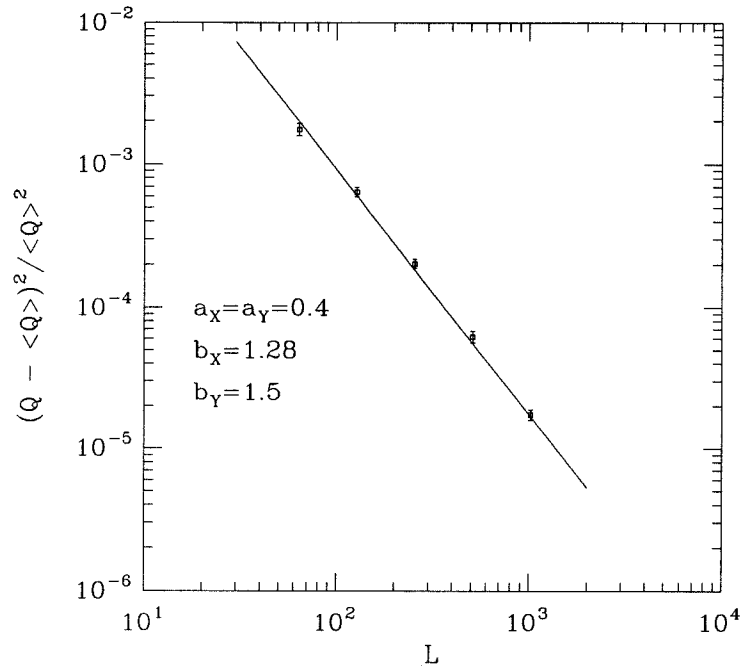

Figure 1-16: Mean square fluctuations as a function of system size.

of the coarse-grained lattice amplitude fluctuations, averaged over N sites, where $1 \ll N \ll L$:

$$\sigma_N = \left\langle \left(\frac{1}{N} \sum_{j=1}^{N} y_j \right)^2 \right\rangle, \tag{1.73}$$

where, for simplicity, we assume the fluctuations are about zero mean. By simple manipulations, σ_N can be related to the structure factor $S(k)$:

$$\sigma_N = \frac{1}{N^2} \frac{1}{L} \sum_{k=0}^{1/2} \frac{\sin^2(\pi N k)}{\sin^2(\pi k)} S(k). \tag{1.74}$$

For model A, $S(k) \sim \sin^2(\pi k)$ (cf. Figure 1-6), and therefore $\sigma_N \sim 1/N^2$. If an entropy function indeed exists, the simple Taylor series approach underlying the Einstein fluctuation theorem appears therefore not to be directly applicable. Model B does not suffer this difficulty because $S(k) \sim const$ (cf. Figure 1-8).

1.6.3 Discussion

In section 1.6.2 we have presented numerical results both in favor and against the existence of a thermodynamic limit of our coupled map models. One of the main problems is how to distinguish partitions of Q due to bulk effects from partitions due to surface effects. As an example how surface effects can occur, we briefly discuss a system that has been suggested as a counterexample to the idea that the division of Q is determined by maximizing a bulk entropy [67].

We again start with two maps X and Y of equal length L, but now we place them alongside each other such that every site in X couples to a corresponding site in Y. The *intra*-lattice dynamics is the same as in model A:

$$y_1^{n+1}(i) = y_1^n(i) + f_1(y_1^n(i+1)) - 2f_1(y_1^n(i)) + f_1(y_1^n(i-1)), \quad (1.75)$$

$$\text{and} \quad y_2^{n+1}(i) = y_2^n(i) + f_2(y_2^n(i+1)) - 2f_2(y_2^n(i)) + f_2(y_2^n(i-1)). \quad (1.76)$$

The *inter*-lattice coupling is introduced by periodically adding the following terms to the equation of motion:

$$y_1^{n+1}(i) = y_1^n(i) + \alpha\{f_2(y_2^n(i)) + f_1(y_1^n(i+1)) - 2f_1(y_1^n(i))\}, \quad (1.77)$$

$$\text{and} \quad y_2^{n+1}(i) = y_2^n(i) + \alpha\{f_1(y_1^n(i)) + f_2(y_2^n(i+1)) - 2f_2(y_2^n(i))\}, \quad (1.78)$$

where α is a constant. It is clear that the inter-lattice coupling violates the parity symmetry $i \leftrightarrow -i$. More important, however, is that a division of Q is likely to occur without any bulk effects being responsible. An easy way to see this is to consider the case where the nonlinear functions f are the sum of a linear and a random term:

$$f_1(x) = a_1 x + b_1 \xi, \quad (1.79)$$

$$f_2(x) = a_2 x + b_2 \xi, \quad (1.80)$$

where the ξ_i on different lattice sites are uncorrelated. Taking the time average of

Eq. (1.77), setting $\langle y_1^n(i)\rangle = q_1$ and $\langle y_2^n(i)\rangle = q_2$, we find that equilibrium is attained when:

$$a_2 q_2 - a_1 q_1 + (b_2 - b_1)\langle \xi \rangle = 0. \tag{1.81}$$

We will therefore quite generally find $q_1 \neq q_2$, and it is obvious that no bulk effects are responsible.

Returning to couplings Eq. (1.71) and Eq. (1.72) investigated in section 1.6.2, we see that they do not have the flaw of the system described above. However, there is another potential problem with these couplings, and we therefore introduce yet another candidate for the flux term between the two systems.

We would expect that in the limit of uncoupled systems (i.e., the coupling strength goes to zero), the coupling operator itself should average to zero. One way to ensure this is to require the coupling term to depend on the local *currents* of the uncoupled system, rather than on the local *amplitudes*. We can implement this by replacing Eq. (1.72) by:

$$\begin{aligned} y_X^{n+1}(L_X) &= y_X^n(L_X) - g_X(y_X^n(L_X),\, y_X^n(L_X - 1)) \\ &\quad + C\left(g_X(y_X^n(L_X), y_X^n(L_X - 1)),\, g_Y(y_Y^n(2), g_Y^n(1))\right), \end{aligned} \tag{1.82}$$

where $C(x, y)$ is an arbitrary function satisfying $C(x, y) = -C(y, x)$ to maintain parity symmetry $i \leftrightarrow -i$.

One difficulty with implementing Eq. (1.82) is that only the nonlinear components of the coupling function $C(x, y)$ can lead to macroscopic currents. In our numerical simulations, we are hampered by large fluctuations, which often cause the coupled maps to enter a periodic orbit. We have therefore not been able to obtain conclusive results with this coupling, although there are indications that equilibrium is established for a different division of Q than for the coupling Eq. (1.71), casting some doubts on our heat bath algorithms.

We have been able to obtain some results for model B, with $C(x, y) = dxy$,

where d is the coupling strength. This coupling does not satisfy parity symmetry, but we believe that in the limit $d \to 0$ the same results as for a parity symmetric coupling should be obtained. We have used these results to investigate a rather speculative question, namely whether the rate of information production should be at an extremum when two maps are in equilibrium. The rate of information production is called the *Kolmogorov entropy* h [26]. It can be shown that the sum of the positive Lyapunov exponents provides an upper bound to h [68], and it is a strong possibility that an equality holds for systems having a physical measure [26]. For a given map, we therefore assume that we can compute h as a function of Q from the Lyapunov spectrum. We then compute h_1 and h_2 for two maps with different map parameters, for conserved quantities Q_1 and $Q_2 = Q_c - Q_1$, where Q_c is fixed. We then plot $h_1 + h_2$ versus $q_1 = Q_1/L$, and check whether the plot shows an extremum at that value of q_1 which arises when the two maps are coupled together with an initial value of Q_c for the conserved quantity. We show one particular result in Figure 1-17, where the initial value of q was 0.5.

The plot shows indeed an extremum for $q_1 \approx 0.68 \pm 0.01$, compared with a value of $q_1 \approx 0.65 \pm 0.03$ observed when the maps were coupled. The large error bars on the latter value are due to the large fluctuations during the evolution of the coupled system. This is qualitatively consistent with Figure 1-17, which shows that $h_1 + h_2$ depends only very weakly on q_1. We emphasize that these results have to be considered as rather speculative, since there is no clear understanding whether the Kolmogorov entropy should take on an extremum. We also have not been able to consistently reproduce the behavior of Figure 1-17 in model A.

1.7 Analysis of an Experiment

We now present a more detailed discussion of the convection experiment by Ciliberto and Bigazzi [9] already mentioned in section 1.1.1 above. Recall that the experiment

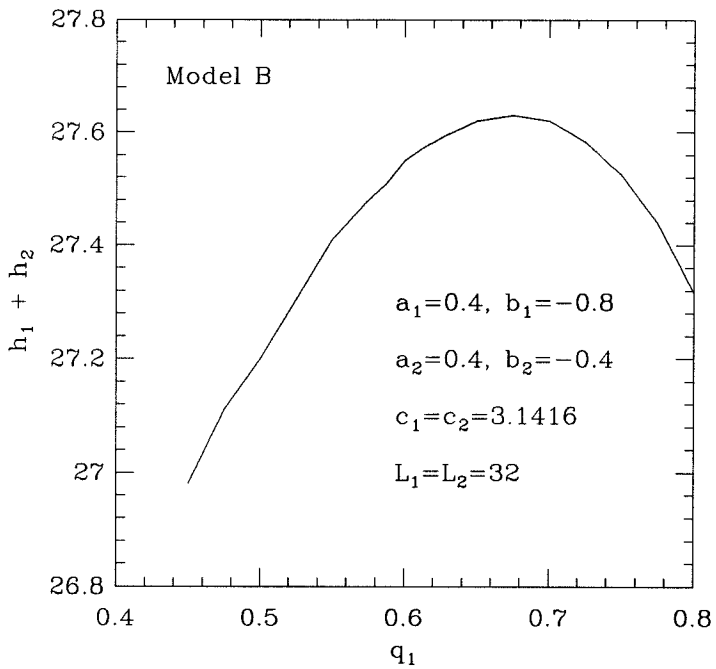

Figure 1-17: Kolmogorov entropy as function of q_1.

consists of convection in an annulus, with convection rolls along the radial direction (cf. Fig. 1-18).

In the experiment, the vertically averaged temperature gradient perpendicular to the radial direction is measured at N equally spaced points located at a fixed radial distance from the center of the cell. N is typically between 128 and 256, and the sampling rate is approximately 1/10 of the oscillation time of one convection roll.

If we denote the experimental measurements as $y^n(i)$, where i labels the position of the probe, and n labels the sampling time, we can interpret $y(i)$ as forming a one-dimensional coupled map lattice, with a discrete time evolution given by the sampling rate. We wish to explore the similarity between this 'lattice' constructed from experimental observations, and the coupled map models we have studied in this chapter. An important difference between the experimental situation and our

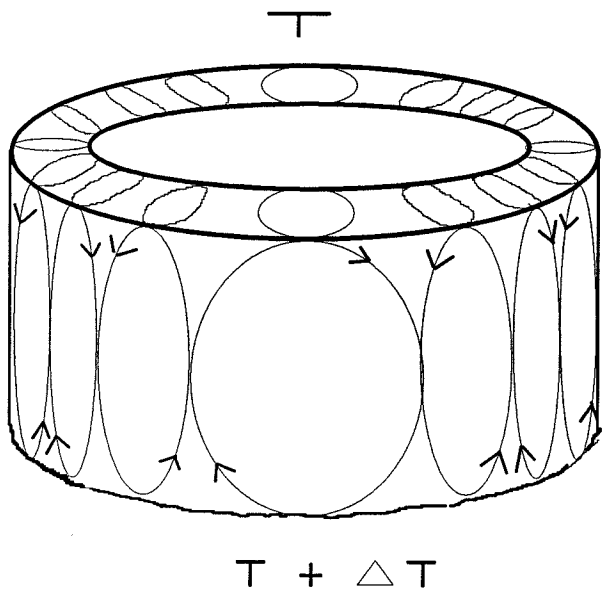

Figure 1-18: Convection experiment in an annulus.

models is that the experimental data points are strongly driven externally by the motion in the whole convection cell, while our models are entirely self-interacting. We assume that the strongly nonlinear map functions in our model can emulate this external driving process.

The experimental $y^n(i)$ also satisfy an approximate conservation law, since the temperature gradient integrated around the cell vanishes. Because of the discrete sampling, this conservation law is only approximate.

In the experiment, the temporal fluctuations of $y^n(i)$ at a fixed position i show a complicated distribution. By contrast, the fluctuations of the Fourier transforms $y^n(k)$ at a fixed wavevector k show approximately a Gaussian distribution in the chaotic regime. This result agrees with our discussion in section 1.3.2 of the applicability of the central limit theorem due to finite correlation lengths. Below the onset of spatiotemporal chaos, the distribution of the $y^n(k)$ is not Gaussian, as we would expect from the spatial periodicity of convection roll patterns at small driving.

Finally, the authors measure quantities they term 'energy' and 'entropy'. The

energy E^n is defined as:

$$E^n = \sum_{i=1}^{N} (y^n(i))^2. \tag{1.83}$$

Using Parseval's theorem, we interpret the time average E of E^n as the static structure factor $S(k)$ summed over k. From our Langevin description of the structure factor in section 1.4, we would therefore expect E to provide a measure of the 'noise' in the system, and to increase with the nonlinearity. In the experiment it is indeed found that in the chaotic regime E increases approximately linearly with the applied vertical temperature gradient.

The entropy σ^n is defined as:

$$\sigma^n = -\frac{1}{\sigma_0} \sum_{k=1}^{N/2} \phi^n(k) \log(\phi^n(k)), \tag{1.84}$$

where $\phi^n(k) = |y^n(k)|^2/E^n$, and $\sigma_0 = \log(N/2)$. A rough interpretation of $\sigma = \langle \sigma^n \rangle$ is as an indicator how equipartitioned the static structure factor $S(k)$ is as a function of k. When the structure factor is a constant independent of k, σ takes on its maximum value of 1, while a structure factor peaked at a single value of k results in the minimum value of 0.

In the chaotic regime, σ is found to remain close to its maximum value, indicating a static structure factor similar to model B. (cf. Figure 1-8). Unfortunately, the authors do not report the dynamic structure factor, which would provide a more stringent test of the Langevin description of section 1.4.

While these observations do not provide rigorous quantitative tests, they do indicate that some of the results obtained with our coupled maps models may apply to physical experiments. Whether our heat bath algorithms of section 1.6.2 can be tested in an actual experiment remains to be elucidated and is certainly worth investigating.

1.8 Conclusion

Our study of coupled maps with conservation laws has led to some interesting results, while at the same time raising several questions which require further investigations. We have derived simple Langevin equations which can adequately describe many long wavelength features of strongly chaotic systems. We have shown why the fluctuation-dissipation theorem will in general not allow the definition of a useful effective temperature in a nonequilibrium system. Finally, we have presented empirical evidence that some ideas from equilibrium thermodynamics may carry over to chaotic systems without an underlying Hamiltonian.

The most important question that our work has not been able to resolve completely is how to conclusively distinguish surface effects from bulk effects in the distribution of a conserved quantity between two chaotic systems. Even if this question can be resolved, and something analogous to the maximum entropy principle of thermodynamics can be established for chaotic systems, one needs to identify experimentally measurable quantities to test these ideas. We have only been able to present rather preliminary results using the Kolmogorov entropy (cf section 1.6.3), which can in principle be measured experimentally.

Appendix

In this appendix we briefly outline the numerical procedures we used to compute Lyapunov exponents. Since in our coupled map models the equations of motion and therefore the Jacobian matrices are known, we could, in principle, use Eq. (1.13) to determine the Lyapunov spectrum. However, this would quickly lead to numerical difficulties due to the exponential divergence of trajectories, which results in singular values of the products of the Jacobians. A better approach consists of following the evolution of an orthonormal set of vectors, which is periodically renormalized to avoid collapse onto the most rapidly growing directions [69, 70]. This can be

accomplished with two mathematically equivalent, but numerically slightly different methods.

In the first method, one starts with a random orthonormal set of vectors, and operates on that set successively with the instantaneous Jacobians. The vectors will therefore start to align themselves along the most rapidly growing directions. One then periodically applies the Gram-Schmidt renormalization to these vectors. During Gram-Schmidt renormalization, the space spanned by the first k vectors is left unchanged, where k ranges from one to the number of vectors available. The Gram-Schmidt procedure therefore replaces an almost degenerate complete set by an equivalent orthonormal one, solving the computational difficulties. The first vector is not rotated at all during renormalization, and can therefore align itself onto the most rapidly growing direction. The second vector is orthogonalized to the first vector, and can therefore only seek the second-most rapidly growing direction. Likewise, each succeeding vector will be orthogonal to all the previous ones. The logarithms of the scale factors needed to normalize the vectors to unit length, averaged over time, converge to the Lyapunov exponents. One potential difficulty with this method is that the Gram-Schmidt procedure gets more and more inaccurate numerically as the number of vectors to be orthonormalized is increased.

The second method is based on the QR algorithm [26] and is numerically more robust. The QR algorithm factors a matrix A into an orthonormal matrix Q, and an upper triangular matrix R. The matrix Q forms an orthonormal basis for A, and is identical to that obtained by the Gram-Schmidt procedure. As in the first method, one starts with a random set of orthonormal vectors, and applies the Jacobian to that set. The resulting matrix is factored according to the QR algorithm, and at each succeeding iteration, the Jacobian is applied to the orthonormal matrix resulting from the previous QR factorization. This generates a sequence of upper triangular matrices, $R_1, R_2, \ldots$. The product of these matrices is also upper triangular, and the logarithms of the diagonal entries, averaged over a large number of R_i, converges

to the Lyapunov exponents. Evidently only the diagonal entries of the R_i need to be kept during simulations. The numerical complexity of both algorithms increases as the cube of the number of exponents computed.

The QR algorithm is computationally slower than the Gram-Schmidt procedure by approximately a factor of two, and for fewer than $\sim$ 50 vectors we have obtained satisfactory results with a modified Gram-Schmidt algorithm [71], without appreciable sacrifice in accuracy.

It is also possible to compute the Lyapunov spectrum from a time series of experimental data [72], although it appears that only the positive exponents can be reliably obtained. The complexity of these algorithms increases exponentially with the dimension, and they are therefore only applicable to low-dimensional attractors.

References

[1] D. J. Tritton, *Physical Fluid Dynamics*, Oxford University Press (1988).

[2] D. Forster, *Hydrodynamic Fluctuations, Broken Symmetry, and Correlation Functions*, W. A. Benjamin Inc. (1975).

[3] P. C. Hohenberg and B. I. Halperin, Rev. Mod. Phys. **49**, 435 (1977), and references therein.

[4] J. L. Lebowitz, Physica **140A**, 232 (1986).

[5] For a review of the early experimental and theoretical work on Rayleigh-Bénard convection, see S. Chandrasekhar, *Hydrodynamic and Hydromagnetic Stability*, Oxford University Press (1961).

[6] A. C. Newell and J. A. Whitehead, J. Fluid. Mech. **38**, 279 (1969).

[7] For an extensive review, see M. C. Cross and P. C. Hohenberg, *Pattern Formation outside of Equilibrium*, to be published in Reviews of Modern Physics.

[8] G. Ahlers and R. P. Behringer, Prog. Theor. Phys. (Kyoto) Suppl. **64**, 186 (1978); J. P. Gollub, A. R. McCarrior, and J. F. Steinmann, J. Fluid Mech. **125**, 259 (1982); S. Ciliberto, J. Phys. Cond. Matter **2**, SA483 (1990).

[9] S. Ciliberto and P. Bigazzi, Phys. Rev. Lett. **60**, 286 (1988).

[10] E. N. Lorenz, J. Atmos. Sci. **20**, 130 (1963).

[11] J. H. Curry, J. R. Herring, J. Loncaric, and S.A. Orszag, J. Fluid Mech. **147**, 1 (1984).

[12] Y. Kuramoto and T. Tsuzuki, Prog. Theor. Phys. **55**, 356 (1976); G. I. Sivashinsky, Acta Astronautica **6**, 569 (1979).

[13] P. Manneville, "Lyapunov exponents for the Kuramoto-Sivashinsky model," in *Macroscopic modeling of turbulent flows*, ed. O. Pironneau, Lect. Notes in Physics **230**, Springer Verlag (1985).

[14] S. Ciliberto and M. Caperoni, Phys. Rev. Lett. **64**, 2775 (1990).

[15] Spatiotemporal intermittency in hydrodynamics refers to the random switching between laminar and turbulent flow. See, e.g., Ref. [1] above, p. 285.

[16] M. Faraday, Phil. Trans. R. Soc. London **121**, 299 (1831).

[17] For a review of parametrically excited surface waves, see J. Miles and D. Henderson, Ann. Rev. Fluid Mech. **22**, 143 (1990).

[18] N. B. Tufillaro, R. Ramshankar, and J. P. Gollub, Phys. Rev. Lett. **62**, 422 (1989). See also J. P. Gollub and R. Ramshankar, "Spatiotemporal chaos in interfacial waves," in *New Perspectives in Turbulence*, ed. L. Sirovich, Springer Verlag (1991).

[19] For a review of maps on the unit interval, see P. Collet and J. P. Eckmann, *Iterated Maps of the Interval as Dynamical Systems*, Birkhäuser, Boston (1980).

[20] For an extensive discussion of the logistic map and its history in modeling population dynamics, see R. M. May, Nature **261**, 459 (1976).

[21] M. J. Feigenbaum, J. Stat. Phys. **19**, 25 (1978), and J. Stat. Phys. **21**, 669 (1979).

[22] Periodic-doubling chaos has been observed in several convection experiments, e.g., J. P. Gollub and S. V. Benson, J. Fluid Mech. **125**, 15 (1980); J. Maurer and A. Libchaber, J. de Phys. Lett. **41**, L515 (1980).

[23] For a review, see N. B. Abraham, J. P. Gollub, and H. L. Swinney, Physica D **11**, 252 (1984).

[24] W. Lauterborn and E. Cramer, Phys. Rev. Lett. **47** 1445 (1981); M. Kitano, T. Yabuzaki, and T. Ogawa, Phys. Rev. Lett. **50**, 713 (1983).

[25] See, e.g., L. Glass, M. R. Guevara, A. Shrier, and R. Perez, Physica D **7**, 89 (1983).

[26] For an introduction to the mathematical foundations of the theory of chaos, see J.-P. Eckmann and D. Ruelle, Rev. Mod. Phys. **57**, 617 (1985).

[27] S. M. Ulam and J. von Neumann, J. Bull. Am. Math. Soc. **53**, 1120 (1947); J. von Neumann, *Collected Works* **5**, 768 (1961).

[28] Physical measures are discussed in Ref. [26], p. 626.

[29] See, e.g., M. Hénon, "Numerical exploration of Hamiltonian systems," in *Chaotic Behavior of Deterministic Systems*, ed. G. Iooss, North-Holland (1983).

[30] V. I. Oseledec, Moscow Math. Soc. **19**, 197 (1968).

[31] B. Mandelbrot, *The Fractal Geometry of Nature*, Freeman, New York (1983).

[32] K. Kaneko, Physica D **37**, 60 (1989) and references therein.

[33] K. Kaneko, Prog. Theor. Phys. **7**, 1033 (1985).

[34] J. D. Keeler and J. D. Farmer, Physica D **23**, 413 (1986).

[35] H. Chaté and P. Manneville, Physica D **32**, 402 (1988).

[36] Y. Pomeau, "Front motion, metastability, and subcritical bifurcations in hydrodynamics," in *Spatio-temporal coherence and chaos in physical systems*, eds. A. R. Bishop, G. Grüner, and B. Nicolaenko, North-Holland (1986); See also Ref. [54] below.

[37] See, e.g., P. Grassberger and T. Schreiber, Physica D **50**, 177 (1991).

[38] L. A. Bunimovich and Y. G. Sinai, Nonlinearity **1**, 491 (1988)

[39] J. P. Crutchfield and K. Kaneko, Phys. Rev. Lett. **60**, 2715 (1988).

[40] T. Bohr, G. Grinstein, Y. He, C. Jayaprakash, Phys. Rev. Lett. **58**, 2155 (1987).

[41] G. Grinstein, Y. He, C. Jayaprakash, and B. Bolker, Phys. Rev. **A44**, 4923 (1991).

[42] H. Sompolinsky, A. Crisanti, and H. J. Sommers, Phys. Rev. Lett. **61**, 259 (1988).

[43] M. S. Bourzutschky and M. C. Cross, Chaos **2**, 178 (1992).

[44] See, e.g., the review by J. P. Crutchfield and J. D. Farmer, Physics Reports **92**, 45 (1982).

[45] B. A. Huberman and J. Rudnick, Phys. Rev. Lett. **45**, 154 (1981).

[46] A. Renyi, *Probability Theory*, North Holland (1970).

[47] J. L. Kaplan and J. A. Yorke, "Chaotic behavior of multi-dimensional difference equations," in *Functional Differential Equations and Approximation of Fixed Points*, eds. H. O. Peitgen and H. O. Walther, *Lect. Notes in Math.* No. **730**, Springer Verlag (1979).

[48] D. Farmer, E. Ott, and J. A. Yorke, J. Diff. Eqns. **49**, 185 (1983).

[49] F. Ledrappier, Comm. Math. Phys. **81**, 229 (1981).

[50] V. N. Shtern, Phys. Lett. **99A**, 268 (1983).

[51] For a detailed discussion of dimension algorithms, see J. Theiler, *Quantifying Chaos: Practical Estimation of the Correlation Dimension*, Ph.D. Thesis, California Institute of Technology 1988 (unpublished).

[52] D. Ruelle, Commun. Math. Phys. **87**, 287 (1982).

[53] P. C. Hohenberg and B. I. Shraiman, Physica D **37**, 109 (1989).

[54] P. Manneville, *Dissipative Structures and Weak Turbulence*, Academic Press (1990).

[55] N. G. Van Kampen, *Stochastic Processes in Physics and Chemistry*, North-Holland (1981).

[56] U. Deker and F. Haake, Phys. Rev. **A11**, 2043 (1975).

[57] R. Graham, "Statistical Theory of Instabilities in Stationary Nonequilibrium Systems with Applications to Lasers and Nonlinear Optics," *Springer Tracts in Modern Physics*, Springer Verlag (1973).

[58] D. Forster, D. R. Nelson, and M. J. Stephen, Phys. Rev. **A16**, 732 (1977).

[59] M. Kardar, G. Parisi, and Y-C. Zhang, Phys. Rev. Lett. **56**, 889 (1986).

[60] S. Zaleski, Physica D **34**, 427 (1989).

[61] H. B. Callen and T. A. Welton, Phys. Rev. **83**, 34 (1951).

[62] C. E. Leith, J. Atmos. Sci. **32**, 2022 (1975).

[63] T. L. Bell, J. Atmos. Sci. **37**, 1700 (1980).

[64] H. B. Callen, *Thermodynamics*, John Wiley & Sons (1961).

[65] For a recent review, see *The dynamic origin of increasing entropy*, M. C. Mackey, Rev. Mod. Phys. **61**, (1989).

[66] See, e.g., L. Landau and E. M. Lifshitz, *Statistical Physics*, Pergamon (1980).

[67] J. Miller, private communication.

[68] Ya. B. Pesin, Russian Math. Survey **32**, 55 (1977).

[69] I. Shimada and T. Nagashima, Prog. Theor. Phys., **61**,1605 (1979); G. Benettin, L. Galgani, and J. M. Streclyn, Phys. Rev. **A14**, 2338 (1976).

[70] A. Wolf, J. B. Swift, H. L. Swinney, and J. A. Vastano, Physica D **16**, 285 (1985).

[71] G. H. Golub and C. F. van Loan, *Matrix Computations*, Johns Hopkins University Press (1989).

[72] J.-P. Eckmann, S. O. Kamphorst, D. Ruelle, and S. Ciliberto, Phys. Rev. **A34**, 4971 (1986); R. Brown, P. Bryant, and H. D. I. Abarbanel, Phys. Rev. **A43**, 2787 (1991); and Ref. [70] above.

Chapter 2

Self-Organized Criticality

An einer Theorie ist es wahrhaftig
nicht ihr geringster Reiz,
daß sie widerlegbar ist:
gerade damit zieht sie feinere Köpfe
an.
F. Nietzsche

2.1 Introduction and Outline

Some of the most interesting and difficult problems in condensed matter physics involve a large range of spatial and/or temporal scales. Quite often in these problems physical variables display *scaling behavior* which can be expressed mathematically by an homogeneity relation. An example is the Gibbs free energy $G(T, H)$ of a magnetic system, when the temperature T approaches a critical temperature T_c at which a second order phase transition occurs. Introducing the reduced temperature $\epsilon = (T - T_c)/T_c$, and letting $G(T, H) \rightarrow G(\epsilon, H)$, it is found [1] that $G(\epsilon, H)$ obeys a generalized homogeneity relation:

$$G(\lambda^{\alpha}\epsilon, \lambda^{\beta}H) = \lambda G(\epsilon, H), \tag{2.1}$$

where α and β are *critical exponents* and λ is an arbitrary parameter. Choosing $\lambda = H^{-1/\beta}$, we find:

$$G(\epsilon, H) = H^{1/\beta} G(\frac{\epsilon}{H^{\alpha/\beta}}, 1), \tag{2.2}$$

so that the Gibbs free energy only depends on the ratio $\epsilon/H^{\alpha/\beta}$, apart from a multiplicative factor. The parameter space is therefore reduced from a function of two variables to a function of one variable, and two critical exponents. Indeed, the critical exponents depend only on the dimensionality and symmetry of the underlying system, not on the details of the microscopic interactions. The fundamental reason for this is that near the critical point the correlation length diverges, which effectively makes other microscopic lengths irrelevant. The renormalization group approach developed by Wilson [2] provides a systematic procedure for computing the critical exponents, with predictions that generally agree quite well with experiment [3]. It is generally believed that the scaling behavior observed can only be achieved by tuning one or more parameters, e.g., the critical temperature T_c.

The situation in nonequilibrium systems is considerably less clear, for example the ubiquitous occurrence of '1/f' noise in situations ranging from resistance fluc-

tuations in semi-conductors to movements in the stock market remains one of the biggest puzzles in science [4]. Motivated by the problem of $1/f$ noise, Bak, Tang, and Wiesenfeld have proposed a class of cellular automata models, referred to as 'sandpiles', because they mimic sand flowing down an incline [5]. Bak et al. argue that these models display what they call *self-organized criticality*, which is quite different from the criticality in equilibrium statistical mechanics: No tuning of parameters is necessary, but the scaling behavior arises instead through the propagation of noise through 'minimally stable' states. Consider, for example, a hypothetical incline on which sand is continuously dropped. Because of friction, the sand can only slide down the incline when the local slope exceeds a certain threshold. When sand actually does slide, it rearranges the distribution of sand on the incline. According to Bak et al., the distribution of sand eventually reaches a minimally stable state where disturbances can propagate arbitrary distances, leading to avalanches of all sizes. Numerical simulations of sandpile models indeed show nontrivial power law distributions, but there is ongoing debate as to whether these power laws really reflect fundamentally new dynamic principles, or whether they can be understood within established frameworks.

Central to the problem of self-organized criticality is the question of under what circumstances scaling behavior can occur. In this chapter we will investigate this question from several different points of view. In Section 2.2 we review the basics of dimensional analysis, which often leads to the prediction of scaling relations with very little theoretical effort. We then describe a simple one-dimensional sandpile model which motivated us to study a piecewise linear diffusion equation, similar to one solved by Barenblatt [6]. We use this equation to show how non-trivial scaling behavior can arise in partial differential equations, with power laws that cannot be obtained by dimensional analysis alone.

In Section 2.3 we focus directly on sandpile models. We start by providing a summary of the extensive research that has been done on self-organized criticality.

We then describe detailed numerical investigations of two particular sandpile models, one with and one without a conservation law. We derive a mean field theory for these models, and comment on the importance of conservation laws and other invariance principles for the self-organized critical state.

In Section 2.4 we investigate the notorious cellular automaton model 'Game of Life' introduced by Conway [7], which has been suggested to show self-organized criticality without an underlying invariance principle [8].

We summarize our results in Section 2.5. In the Appendix we provide an elementary introduction to Boolean algebra and describe efficient computational algorithms for the simulation of cellular automata.

2.2 Nonlinear Diffusion: A Simple Example

2.2.1 Dimensional Analysis and Scaling

Dimensional analysis plays an important part in both experimental and theoretical science. Measurements of physical quantities are always expressed as ratios with certain fundamental units. The complete set of fundamental units used to describe a given class of phenomena is the system of units of measurement. For example, the Système International (SI) standard provides a set of units to measure all physical phenomena deemed worth measuring. Evidently the definition of the fundamental units is quite arbitrary and is usually dictated by convenience [9]. However, once a system of units has been chosen, the units of any physical quantity are products of powers of the fundamental units, independent of the magnitude of those units. For example, the unit of force in the SI system is MLT^{-2}, where M, L, and T are the fundamental units of mass, length, and time respectively. This is true whether one measures mass in kilograms (as in the MKS system) or in grams (as in the cgs system). The MKS and the cgs system really belong to the same class of units, namely the class that takes M, L, and T as the fundamental units.

The subject of dimensional analysis derives mainly from the observation that the unit of a physical quantity is always expressible as a product of powers of the fundamental units. Any physical measurement consists of establishing functional relations of the form:

$$a = f(a_1, a_2, \ldots, a_k, a_{k+1}, \ldots, a_n), \tag{2.3}$$

where the quantities $a_1, \ldots, a_n$ are called the *governing parameters* of a [6]. Of these n parameters, in general only a subset consisting of k members $a_1, \ldots, a_k$ will have independent dimensions. The dimensions of the quantity a, and the dimensions of the quantities $a_{k+1}, \ldots, a_n$, can then be expressed as products of powers of the dimensions of the members of that subset. Using this information, one can then introduce dimensionless ratios by dividing a, $a_{k+1}, \ldots, a_n$ by appropriate products of $a_1, \ldots, a_k$. Let these dimensionless ratios be Π, $\Pi_1, \ldots, \Pi_{n-k}$. Then the Buckingham Pi theorem [10] states that there exists a function F such that:

$$\Pi = F(\Pi_1, \ldots, \Pi_{n-k}). \tag{2.4}$$

As a famous example to illustrate the Pi theorem, we briefly describe how G.I. Taylor deduced the energy released in a nuclear explosion from a set of pictures showing the radius of the fireball at several instants in time [11]. He assumed that the radius r of the fireball depends mainly on the energy of the explosion E, time t, and the ambient air density ρ:

$$r = r(E, t, \rho). \tag{2.5}$$

The dimensions of E, t, and ρ are ML^2T^{-2}, T, and ML^{-3} respectively. Obviously these dimensions are all independent, and from the Pi theorem we deduce that the right hand side of Eq. (2.4) is a simple constant in this case, since $n - k = 0$. By

forming the product of E, t, and ρ that has the dimension of length we obtain:

$$r/(Et^2/\rho)^{1/5} = C, \tag{2.6}$$

where C is a constant. Plotting $\log(r)$ vs. $\log(t)$ one should thus obtain a slope of $2/5$, as was indeed observed [11]. In order to obtain the actual energy E, however, one also needs to know the proportionality constant C. The big advantage of a scaling relation like Eq. (2.6) is that no reference is made to the actual size of the explosion. We then expect the constant C to be same in a nuclear explosion as in a conventional chemical explosion, and that is indeed how Taylor deduced the energy.

There are of course several caveats in applying dimensional analysis, since the choice of governing parameters usually cannot be deduced from first principles. For example, in the analysis of the nuclear explosion above, there is no a priori reason not to include the linear dimension l of the bomb itself as one of the governing parameters. Applying the Pi theorem, we then find that the right hand side of Eq. (2.6) is no longer a simple constant, but an *arbitrary function* of the ratio $l/(Et^2/\rho)^{1/5}$. Our intuition is that this ratio is 'small' and that we can let it go to zero, making the arbitrary function a constant. In general this cannot be rigorously justified, since the limit $x \to 0$ of an arbitrary function $f(x)$ may not exist. Indeed, non-trivial scaling relations, which cannot be deduced from dimensional analysis alone, can arise precisely because of subtleties in taking such limits [6].

Another simple example, which will be the starting point of the more complicated problem discussed in section 2.2.3, is provided by the one-dimensional linear diffusion equation

$$\partial_t y(x,t) = D\partial_x^2 y(x,t), \tag{2.7}$$

$$y(x,0) = Q\delta(x). \tag{2.8}$$

Here D is the diffusion constant, and the domain x is unbounded. The parameters

x, t, D, and Q have dimensions L, T, L^2/T, and EL respectively, where we have assigned y an arbitrary dimension of E. Only three of the four parameters have independent dimensions, and applying the Pi theorem we find that y should be of the form

$$y(x,t) = \frac{Q}{\sqrt{Dt}} f(x/\sqrt{Dt}), \tag{2.9}$$

where f is an arbitrary function. Substituting Eq. (2.9) into Eq. (2.7) we obtain an ordinary differential equation for $f(\eta)$ in the single variable $\eta = x/\sqrt{Dt}$:

$$f'' + \frac{1}{2}\eta f' + \frac{1}{2} f = 0. \tag{2.10}$$

The solution which vanishes at infinity is evidently

$$f(\eta) = A \exp(-\frac{1}{4}\eta^2), \tag{2.11}$$

where A is at this stage an arbitrary constant. The complete solution to Eq. (2.7) is now easily found to be

$$y(x,t) = \frac{1}{2}\frac{Q}{\sqrt{\pi Dt}} \exp(-\frac{1}{4}\frac{x^2}{Dt}), \tag{2.12}$$

which is of course the well known solution to the linear diffusion equation with an impulsive initial condition. The main advantage of dimensional analysis in this simple example was the reduction of a partial differential equation to an ordinary differential equation. As in the example of the nuclear explosion above, we expect the general scaling form Eq. (2.9) to remain valid in the long time limit, even if the initial condition is not a delta function, but spread over some distance l. Again this corresponds to assuming that the additional dimensionless ratio $l/\sqrt{Dt}$ becomes irrelevant for small l and large t.

The time dependent prefactor of Eq. (2.9) will in general depend on the initial conditions. In section 2.2.3 below we will attempt to analyze the behavior of a

diffusive system in a semi-infinite domain with vanishing slope at the origin and a vanishing spatial integral. The expected scaling form is then not $t^{-1/2}f(x/\sqrt{t})$, but rather $t^{-3/2}f(x/\sqrt{t})$.

We now describe the 'local limited' sandpile model, our motivation for studying a simple nonlinear version of the linear diffusion equation considered above.

2.2.2 The Local Limited Model

The local limited model is a one-dimensional cellular automaton, with rules which are very similar to many of the sandpile models studied for self-organized criticality [13, 12]. The model consists of integral variables $h(i)$, arranged on a one-dimensional lattice indexed by i, where i ranges from 1 to the system size L. The integer $h(i)$ can be interpreted as the number of 'sand grains' at position i, where each grain has a height of unity. The local slope $\sigma(i)$ is defined by the height difference between two nearest neighbors

$$\sigma(i) = h(i) - h(i+1). \tag{2.13}$$

The boundary conditions are

$$\sigma(0) = 0 \tag{2.14}$$

$$h(i) = 0 \quad \text{for } i > L. \tag{2.15}$$

The dynamics consists of randomly selecting a site i and adding a sand grain by incrementing $h(i)$. If the local slope $\sigma(i)$ exceeds a threshold value σ_c, an 'avalanche' is initiated by the process:

$$h(i) = h(i) - n \tag{2.16}$$

$$h(i+1) = h(i+1) + n, \tag{2.17}$$

where n is an integer (if $i = L$, n grains drop off the pile and $h(L+1)$ is kept at zero). Eq. (2.16) is then applied repeatedly to all lattice sites that exceed the threshold until all the local slopes are below or equal to σ_c.

Several interesting quantities can then be measured for this model, for example the distribution of sand leaving the system at $i = L$, and the distribution of the number of sites participating in an avalanche. Extensive numerical simulations indicate that these quantities may have multi-fractal distributions [13, 14].

It is convenient to recast the entire dynamics in terms of the slope variables $\sigma(i)$ alone. Dropping a sand grain corresponds to a distortion in the slope, but the sum of the local slopes over the system remains unchanged. The dynamics when the threshold σ_c is exceeded becomes

$$\sigma(i) = \sigma(i) - 2n, \tag{2.18}$$

$$\sigma(i\pm1) = \sigma(i\pm1) + n, \tag{2.19}$$

which is very much like a discretized diffusion equation.

As our model system we will now take the equation:

$$\begin{aligned} \partial_t y(x,t) &= D\partial_x^2 y(x,t), \qquad (2.20)\\ D &= 1 \quad \text{for } y > 0 \\ D &= 1-\epsilon \quad \text{for } y < 0. \end{aligned}$$

We interpret y as being similar to the slope variable in the local limited model, and we have implemented the nonlinear threshold condition by the discontinuous diffusion coefficient D. We will be interested in the decay of initial conditions corresponding to a local distortion of y, e.g., taking the form of a single period of a sine wave. It is clear that Eq. (2.20) is nonlinear for $\epsilon \neq 0$, and one may even question the existence of a solution. A theorem by Kamenomostskaya [15], however, guarantees the existence of solutions which are both continuous and have continuous

first derivatives.

We should emphasize that Eq. (2.20) cannot be considered as a good description of the local limited model, but is rather an attempt to capture features which may be relevant in similar models. For example, it can be shown that avalanches in the local limited model always terminate at 'troughs', which are sites where the local slope $\sigma(i)$ satisfies $\sigma(i) \leq \sigma_c - n$ [12]. Numerically, it is found that the density of such troughs scales with the system size as $L^{-1/3}$. The trough dynamics are clearly not captured in Eq. (2.20). Some of the consequences of the trough dynamics are analyzed in [16].

2.2.3 The Barenblatt Equation

Barenblatt [6] has studied an equation very similar to Eq. (2.20), and we will therefore refer to Eq. (2.20) and similar piecewise linear diffusion equations as *Barenblatt equations.* Barenblatt considered the case where the diffusion coefficient D is a discontinuous function of ${\partial_x}^2 y$, rather than y itself, and where the initial condition is a simple pulse rather than the sine pulse considered here. The Barenblatt equation has also been used to illustrate singular perturbation theory, if one tries to expand about $\epsilon = 0$ [17].

Let us first consider the trivial case $\epsilon = 0$. As indicated in the previous section, we expect scaling solutions of the form $t^{-3/2} f(x/\sqrt{t})$. This is most easily seen from the exact solution for arbitrary initial conditions and zero slope at the origin:

$$y(x,t) = \frac{1}{2\sqrt{\pi t}} \int_0^\infty d\xi u(\xi) \{\exp(-(\xi+x)^2/4t) + \exp(-(\xi-x)^2/4t)\} \quad (2.21)$$

$$u(x) = y(x,0). \quad (2.22)$$

If $u(x)$ falls off fast enough as $x \to \infty$, we can obtain the asymptotic solution for large t by expanding the exponentials. Requiring the spatial integral of u to vanish, we directly obtain the desired scaling form.

Consider now the case $\epsilon \neq 0$. Applying dimensional analysis naïvely, we would expect a scaling solution of the form:

$$y(x,t) = t^{-3/2} f(x/\sqrt{t}, \epsilon). \tag{2.23}$$

Substituting this ansatz into Eq. (2.20) we obtain an ordinary differential equation for f in terms of the single variable $\eta = x/\sqrt{t}$

$$Df'' + \frac{1}{2}\eta f' + \frac{3}{2} f = 0. \tag{2.24}$$

We now need to separately solve the cases $f < 0$ and $f > 0$ and match the solutions at $f = 0$. The solution to Eq. (2.24) which is positive and has zero slope at the origin can be expressed in terms of a parabolic cylinder function U [18]:

$$f(\eta) = -A \exp(-\eta^2/8) U(-5/2, \eta/\sqrt{2}), \tag{2.25}$$

where A is a constant. Similarly, the negative solution to Eq. (2.24) which goes to zero as $\eta \to \infty$ is:

$$f(\eta) = B \exp(-\frac{\eta^2}{8(1-\epsilon)}) U(-5/2, \eta/\sqrt{2(1-\epsilon)}), \tag{2.26}$$

where B is a constant. To match the solutions we need to locate a common zero of Eq. (2.25) and Eq. (2.26). However, since $U(-5/2, x)$ has only one zero [18], there is no common solution unless $\epsilon = 0$. We conclude that there are no scaling solutions of the form assumed in Eq. (2.23).

Surprisingly, a scaling solution is still possible. Indeed, we need to reexamine our assumption that we can neglect the spatial extent l of the initial condition. In our previous analysis, we have assumed that the scaling function $f(x/\sqrt{t}, l/\sqrt{t}, \epsilon)$ will become independent of l in the limit of large t and small l. Another possibility, however, is that f is a singular function of l, taking on the form $f \sim (l/\sqrt{t})^{-\alpha}$,

with α being an arbitrary exponent which cannot be determined from dimensional analysis alone. We then write our new scaling ansatz as:

$$y(x,t) = t^{-\frac{3}{2}(1+\alpha)} f(x/\sqrt{t}). \tag{2.27}$$

The differential equation for f then becomes:

$$f'' + \frac{1}{2}\eta f' + \frac{3}{2}(1+\alpha)f = 0. \tag{2.28}$$

We now follow the same procedure of matching solutions for $f > 0$ and $f < 0$. The solution for $f > 0$ having zero slope at the origin can be expressed in terms of a confluent hypergeometric function M [18]:

$$f(\eta) = M(3(1+\alpha)/2,\ 1/2,\ -\eta^2/4), \tag{2.29}$$

where we have fixed an arbitrary overall normalization by setting $f(0) = 1$. The solution for $f < 0$ which goes to zero as $\eta \to \infty$ is now:

$$f(\eta) = A \exp(-\frac{\eta^2}{8(1-\epsilon)}) U(-3\alpha - 5/2,\ \eta/\sqrt{2(1-\epsilon)}). \tag{2.30}$$

Solving $f(\eta_0) = 0$ simultaneously for both Eq. (2.29) and Eq. (2.30) then leads to the following nonlinear eigenvalue problem:

$$M(3(1+\alpha)/2,\ 1/2,\ -\eta_0^2/4) = 0 \tag{2.31}$$

$$U(-3\alpha - 5/2,\ \eta_0/\sqrt{2(1-\epsilon)}) = 0. \tag{2.32}$$

Once α and η_0 are determined for a given ϵ, the constant A in Eq. (2.30) is fixed by requiring continuity of the first derivatives of f.

In Figure 2-1 we plot the numerical solutions to Eq. (2.31) and Eq. (2.32).

The solutions for $0 < \epsilon < 1$ are unique, and α increases monotonically with ϵ. To

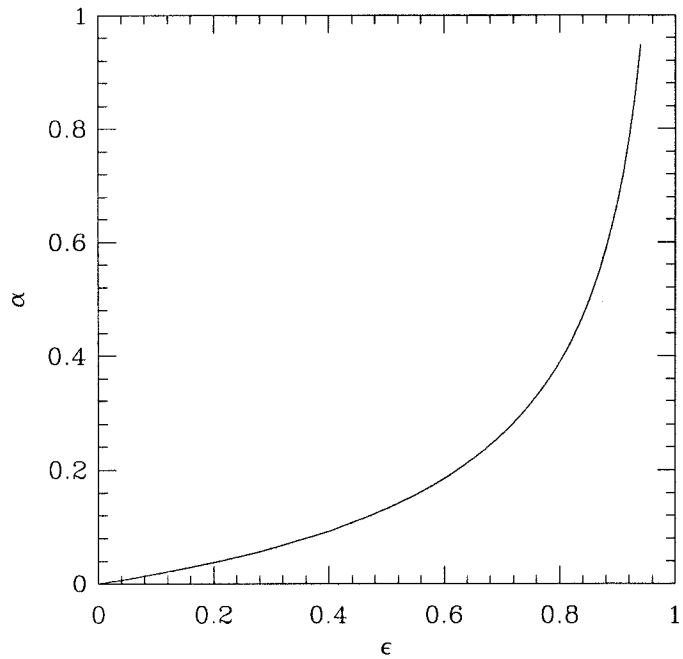

Figure 2-1: Solution to nonlinear eigenvalue problem.

rigorously prove that the scaling solution so obtained is an attractor for arbitrary initial conditions appears very difficult. We limit ourselves to a simple numerical simulation, where we integrate the nonlinear equations for $\epsilon = 0.5$ and the initial condition $y(x,0) = 1$ for $0 < x < 1$, and $y(x,0) = -1$ for $1 < x < 2$. In Figure 2-2 we plot $y(0,t)$ vs. t, which clearly shows a power law decay from which we deduce $\alpha = 0.132 \pm 0.002$, in excellent agreement with $\alpha = 0.1324$ determined from Eq. (2.31).

We have also verified that the solution $y(x,t)$ rapidly approaches the scaling form Eq. (2.27), for several initial conditions.

To summarize, we have found scaling solutions to a simple nonlinear diffusion equation, with a non-trivial exponent determined by solving a nonlinear eigenvalue problem. As in the linear diffusion case, the scaling form corresponds to the solution for a particular initial condition, which acts as an attractor for a large class of other

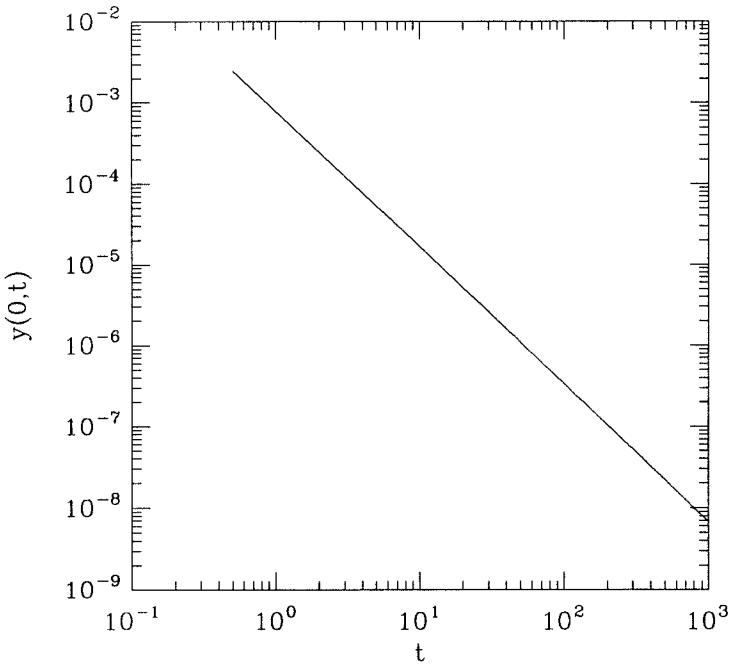

Figure 2-2: Anomalous exponent in nonlinear diffusion equation.

initial conditions. In the linear case, this initial condition is simply a delta function, for the nonlinear case, this initial condition is more complicated. It should be emphasized that the conservation law was not important in arriving at the scaling form.

2.3 Sandpile Models

2.3.1 Background

Sandpile models were introduced by Bak, Tang, and Wiesenfeld [5] who believe them to be simple model systems that display self-organized criticality. The original sandpile models are defined as d-dimensional hypercubic lattices of size L^d, where each lattice site $z_i, i = 1, ..., L^d$, takes on a discrete set of positive integral values. The integer z_i is referred to as the number of 'sand grains' at site i. When $z_i < 2d$,

the site i is called stable. The dynamics is defined by the rules:

1. When the configuration is stable, i.e., all $z_i < 2d$, a site i is selected at random and z_i is incremented, $z_i \rightarrow z_i + 1$.

2. If the configuration is unstable, then synchronously for each unstable site z_i we apply the rule:

$$\begin{aligned} z_i &\rightarrow z_i - 2d, \\ z_j &\rightarrow z_j + 1 \end{aligned}$$

where j ranges over the nearest neighbors of i. We will refer to the application of Rule 2 to a given site i as a 'toppling' event. The boundary conditions are typically chosen such that if j falls outside the lattice, the corresponding sand grain is 'lost'. Rule 2 is applied until all sites are stable, after which a sand grain is added again randomly, using Rule 1. Because sand grains can 'fall off' at the boundary, the number of grains in the lattice will remain bounded.

The event of adding a sand grain and relaxing the lattice to equilibrium will be referred to as an 'avalanche'. For each avalanche, the following quantities can be defined. The 'flip number' F is the total number of toppling events during an avalanche. The 'size' S is the number of distinct sites that topple during an avalanche. Because a given site can topple more than once during a single avalanche, we evidently have $S \leq F$. Finally we define the 'duration' T of an avalanche as the number of synchronous updates required by Rule 2 to relax the lattice to a stable equilibrium configuration.

Extensive computer simulations by numerous groups [19] have clearly established that the distribution functions $D(F)$, $D(S)$, and $D(T)$ have power law forms for large system sizes L. In Figure 2-3 we show $D(F)$ for two-dimensional lattices of several system sizes. Defining the 'toppling exponent' τ by the relation $D(F) \sim F^{1-\tau}$, we find $\tau \approx 2.12 \pm 0.05$, in agreement with other investigations [20].

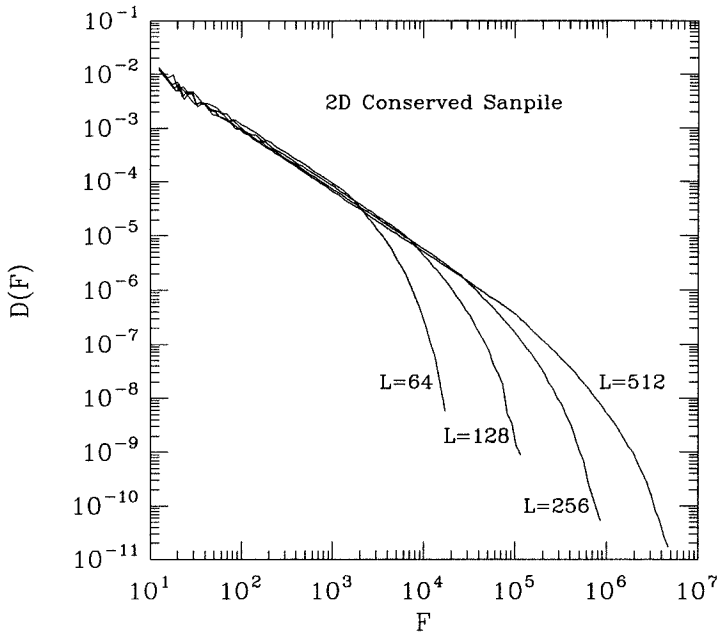

Figure 2-3: Distribution of flip number for 2D conserved sandpile model.

Various modifications and generalizations of the sandpile models have been considered in the literature and we give only a brief summary of those which, we believe, lead to the most important quantitative differences. Among the sandpile models, there seems to be clear differentiation between those operating in one spatial dimension, and those operating in higher dimensions. In fact, the sandpile model described above leads, in one dimension, to a trivial critical state where all sites assume value one. Nontrivial behavior in one-dimensional models is only observed for more complicated rules, such as the local limited model described in section 2.2.2. These one-dimensional models generally do not show simple power laws, but more complicated distributions, which may be multi-fractal [13, 14]. For a particular one-dimensional model it has been shown that the dynamics can be mapped to a nonlinear diffusion equation, where the diffusion coefficient diverges as a power of the system size [21].

As has been pointed out by Dhar [22] the sandpile model defined above has an *Abelian* property, in that the final equilibrium configuration reached after a set of perturbations does not depend on the order in which the perturbations are applied. Using the Abelian property, it can be shown [22] that after an initial transient, the configuration space of the lattice consists of a set of recurrent configurations, which all occur with equal probability. The number of recurrent configurations diverges exponentially with the number of lattice sites N, but is somewhat less than the total number of stable configurations $(2d)^N$. Dhar has also shown that the expectation value of the flip number F obeys the relation $\langle F \rangle \sim L^2$ in arbitrary dimensions [22]. However, even with the Abelian property no explicit expressions for the exponents have been obtained.

The Abelian property is easily destroyed, for example, by toppling rules that depend on the local slope, rather than the local height. Examples of such models have been considered in [13] and [23]; such models usually display power-law behavior as well, but with different exponents. In sections 2.3.2 and 2.3.3 we will study a sandpile model which violates the local conservation law and is not Abelian.

Experimental work on real sandpiles [24, 25] usually shows dynamic behavior which is too complex to be described by simple power laws. Large fluctuations in avalanche sizes have been observed under certain conditions [26] but the precise nature of those conditions and how they may relate to the sandpile models has not been elucidated.

There have been a number of theoretical approaches to the sandpile models, but apart from Dhar's work on Abelian sandpiles [22], none have led to conclusive results. One of the difficulties is that there seems to be little universality in the exponents observed for different models. Another problem is that the concept of an avalanche is difficult to define within the context of a continuum field theory. To illustrate these difficulties, we briefly review the work by Hwa and Kardar [27], which has motivated extensive research using similar approaches [28, 29, 30].

Hwa and Kardar [27] construct a continuum model of a sandpile that incorporates several symmetry considerations. Sand flows in a preferred 'downhill' direction, while the system is translationally invariant in the transverse direction. Sand is locally conserved, except for the external driving, which is assumed to take the form of an uncorrelated Gaussian noise source. Using these considerations, Hwa and Kardar [27] argue that the simplest equation for the fluctuations h of the slope of the sandpile about is critical slope is:

$$\partial_t h(\mathbf{x},t) = \nu_{\|}\partial_{\|}^2 h + \nu_{\perp}\nabla_{\perp}^2 h - \frac{\lambda}{2}\partial_{\|}h^2 + \eta(\mathbf{x},t), \tag{2.33}$$

where the first terms describe relaxation of the height through surface tension, split into two parts perpendicular and parallel to the transport direction. η is a Gaussian noise term with zero mean and second moment:

$$\langle \eta(\mathbf{x},t)\eta(\mathbf{x}',t')\rangle = 2D\delta^d(\mathbf{x}-\mathbf{x}')\delta(t-t'), \tag{2.34}$$

where D is the noise amplitude. In the long wavelength limit, the two-point correlation function $C(\mathbf{x}-\mathbf{x}',t-t') = \langle h(\mathbf{x},t)h(\mathbf{x}',t')\rangle$ is assumed to take the form:

$$C(\mathbf{x},t) = x_{\|}^{2\xi} F(\frac{t}{x_{\|}^z}, \frac{x_{\perp}}{x_{\|}^{\zeta}}) \tag{2.35}$$

where ξ, z, and ζ are the roughness, dynamic, and anisotropy exponents respectively. Using the dynamic renormalization group [31], the exponents for Eq. (2.33) can in fact be determined exactly. Above a critical dimension of $d = 4$, the nonlinear term in Eq. (2.33) becomes irrelevant and ordinary diffusive behavior with $z = 2$ is obtained.

Note that the symmetries incorporated into Eq. (2.33) are quite different from those of the original sandpile model. In particular, the original model does not have a preferred direction. Nevertheless, an exact solution for a particular directed

sandpile model is known [32], with predictions that deviate considerably from those obtained from Eq. (2.33).

There have been several attempts to modify Eq. (2.33) to incorporate the correct symmetries of the various sandpile models [28, 29] but none have led to reliable qualitative predictions. Another problem with trying to apply Eq. (2.33) is that the effective noise term in the original sandpile models may have complicated temporal correlations. The effect of these correlations has indeed been considered [33] but again no definite results have been established.

We conclude that while noisy diffusion equations of the form Eq. (2.33) are interesting models in their own right, they may not provide reliable information about the sandpile models. In particular, the question of which invariance principles, if any, are at work in the sandpile models probably needs to be approached from a different point of view. We will present such a view in section 2.3.2 and discuss our numerical work in section 2.3.3.

2.3.2 Mean Field Theory

For complicated many-body problems, useful insights can often be obtained from mean field theories, in which correlations are ignored. In the context of second order phase transitions mean field theories usually give correct results above a *critical dimension* d_c. The mean field limit of noisy diffusion equations like Eq. (2.33) corresponds to neglecting the nonlinear terms.

Tang and Bak [34] have obtained a mean field theory for sandpiles by assuming that neighboring sites in the lattice are independent. This leads to an evolution equation of the average lattice amplitude, including a random term due to the driving. The validity of the approach by Tang and Bak has been questioned in [35], where the importance of edge effects is emphasized, since sand can only be lost through the edges. Furthermore, the approach in [34] does not lead to a direct prediction of the exponents.

In our mean field theory we will assume that within a given avalanche, each toppling event leads to its own independent avalanche. This is equivalent to assuming that during any toppling, sand grains are not dropped to the nearest neighbors, but to sites arbitrarily far away. Mathematically, this leads to the well-known subject of *branching processes* [36], originally developed to study the fate of family trees in the British aristocracy [37].

In the following discussion, we will refer to the grains that are being dropped due to topplings as *children*. Let $Z_0, Z_1, Z_2, \ldots$ denote the number of children at successive generations, where each generation corresponds to a synchronous update of the lattice. We have $Z_0 = 1$, since the first child is simply the initial grain added to the lattice. Let each toppling event generate Z children and let p be the probability that a child causes another toppling event. By our assumption of independence, p is the same for each child at every generation. The average number of children m that a single child will have is then obviously given by $m = pZ$. If $m < 1$, then each child will have less than one child on average, and it can be shown rigorously [36] that the avalanche will die out in a finite number of steps with probability one. On the other hand, if $m > 1$, there is a finite probability that the avalanche will last forever, i.e., none of the Z_n is zero for arbitrarily large n.

We now suggest that the borderline situation of $m = 1$ is precisely the 'critical point' of the avalanche dynamics. This critical point should be quite independent of how the avalanche actually takes place, in particular, we do not expect local conservation laws to play a significant role. The only assumption is that the system is homogeneous, so that the probability p is indeed the same for each child.

For the special case $m = 1$, several results have been obtained for branching processes, which we can use to determine the flip number exponent τ, and the duration exponent y, defined by the relation $D(T) \sim T^{-y}$. The flip number distribution $D(F)$ is evidently just the distribution of $F = Z_0 + Z_1 + \cdots$. It was shown by Otter [38]

that:

$$D(F = r) \sim r^{-3/2}, \qquad r \to \infty, \tag{2.36}$$

from which we immediately deduce $\tau = 3/2 + 1 = 5/2$. Finally, it was shown by Kolmogorov [39] that the extinction probability $P(Z_n = 0) \sim 1/n$ for large n. Since the extinction probability is the cumulative distribution function of the relaxation times, we deduce that $y = 2$. These predictions agree with exact solutions of the sandpile model on a Bethe lattice [40]. In section 2.3.3 below we present numerical evidence that a sandpile without conservation law or other obvious invariance principles shows criticality, and we compare its behavior with the corresponding conserved model.

2.3.3 Numerical Simulations

The non-conserved model we will investigate has almost the same equations of motion as the conserved model described in section 2.3.1. The rules are [41]:

1. When the configuration is stable, i.e., all $z_i < 2d$, a site i is selected at random and z_i is incremented, $z_i \to z_i + 1$.

2. If the configuration is unstable

$$\begin{aligned} z_i &\to 0 \\ z_j &\to z_j + 1. \end{aligned}$$

Evidently only Rule 2 is different from the conserved model. When a toppling site has more than $2d$ grains, $z_i - 2d$ grains are lost from the system.

In Figure 2-4 we show the flip number distribution for two-dimensional lattices. We clearly observe a power law, from which we deduce $\tau \approx 2.44 \pm 0.02$. While this result is very close to the value $\tau = 2.5$ predicted by mean field theory, we find numerically that the exponent $y \approx 1.68 \pm 0.05$ (cf. Figure 2-5), quite different from

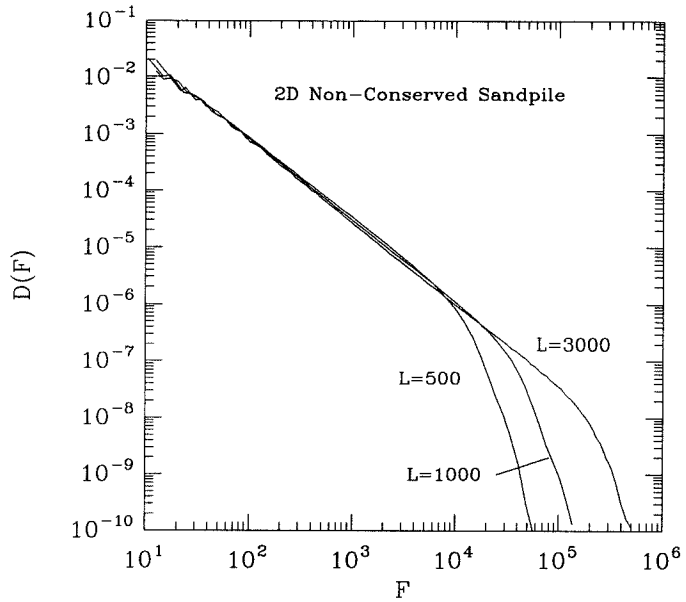

Figure 2-4: Distribution of flip number for 2D non-conserved sandpile model.

the mean field value $y = 2$.

The exponents of the non-conserved model are thus quite different from those of the conserved model, which has $\tau \approx 2.12$ and $y \approx 1.18$ [19].

Comparing Figures 2-3 and 2-4 it is also clear that considerably larger system sizes are needed in the non-conserved model to observe criticality. We can trace some of this behavior to the differences in space-time dynamics between the conserved and non-conserved models. In Figure 2-6 we show the duration T of an avalanche as a function of the linear extent D of the avalanche. We find that $T \approx D^{\zeta}$ with $\zeta \approx 1$. This suggests that avalanches in the non-conserved model are very anisotropic. For computer simulations, this result indicates that finite size effects will be much more pronounced than in a system whose behavior is closer to ordinary diffusion with $\zeta = 2$. For the conserved model, one finds $\zeta \approx 1.5$ [42].

As with the theory of critical phenomena, we expect sandpile models to approach the mean field limit as the spatial dimension is increased, because avalanches will

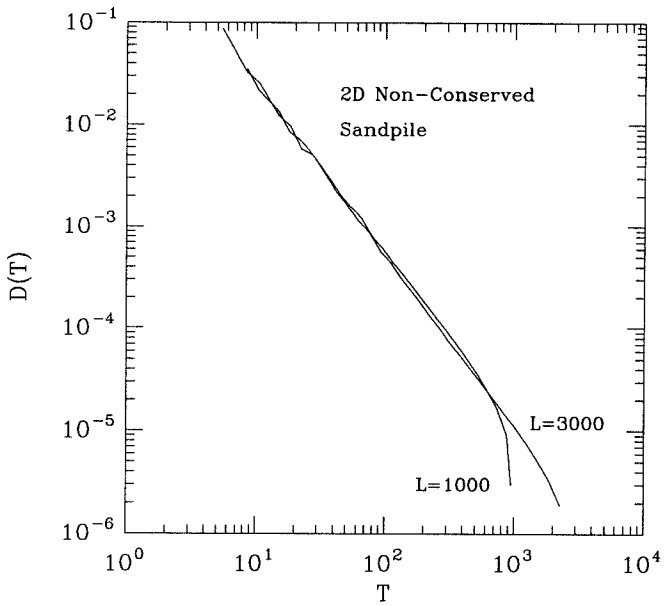

Figure 2-5: Distribution of relaxation times for 2D non-conserved sandpile model.

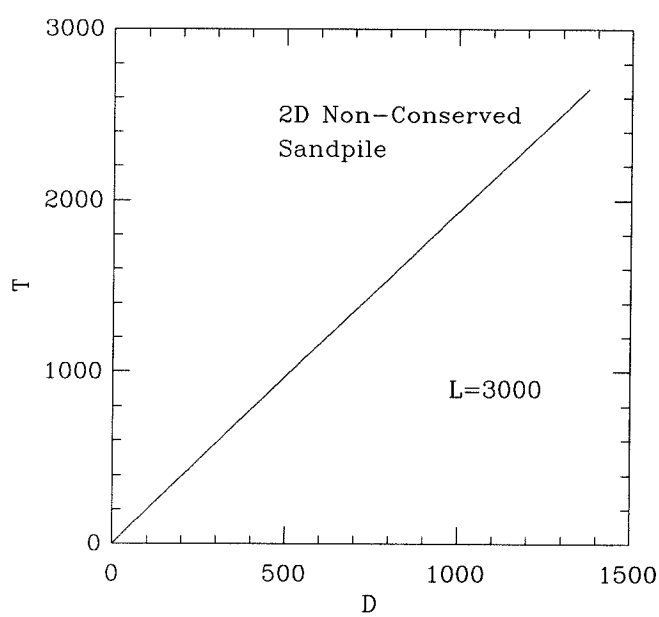

Figure 2-6: Duration of avalanches as a function of linear extent for 2D non-conserved sandpile model.

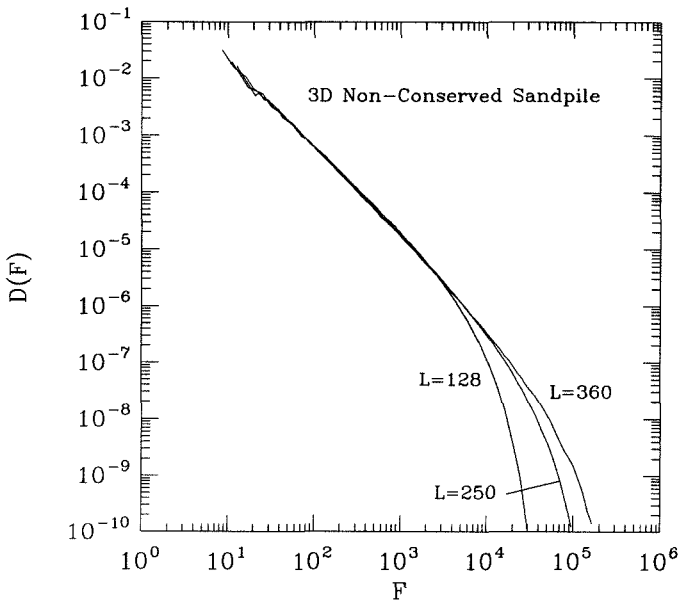

Figure 2-7: Distribution of flip number for 3D non-conserved sandpile model.

be 'less interacting' due to the number of different directions available to them. In critical phenomena, the mean field limit is usually reached at finite upper dimension d_c, which is typically four or six. Whether there exists an upper critical dimension for sandpile models is not clear at present. For the conserved model, numerical results for $d = 4$ [19] are quite close to the mean field exponents derived here. It has been claimed that the exponents are different for $d = 5$ [42], but only very small systems could be simulated casting some doubt on these predictions. Our own investigations are hampered by finite size effects as well, and even for $d = 3$ we cannot obtain very accurate results. In Figure 2-7 we show the flip number distribution for three-dimensional lattices. It is clearly very difficult to obtain a precise exponent from these data: we estimate $\tau \approx 1.50 \pm 0.20$. We therefore do not have enough numerical resolution to determine whether in large enough dimensions the mean field exponents are obtained.

To summarize, we have shown that critical fluctuations can occur in models that do not have an obvious invariance principle in their equations of motion. We have presented a very simple mean field theory, which predicts exponents roughly consistent with those seen in computer simulations of conserved models of sandpiles in four dimensions. For the non-conserved sandpile model, the exponents obtained in two dimensions are very close, but not quite equal to the mean field predictions. We do not have sufficient computer power to obtain conclusive results for our non-conserved model in higher dimensions.

2.4 The Game of Life

2.4.1 Cellular Automata

Cellular automata were introduced by John von Neumann [43] as simplified computational models for biological systems. The main defining characteristic of a cellular automaton model is that it consists of a discrete lattice of cells, where each cell can only take on a discrete set of values [44]. An equation of motion is defined in discrete time, where all lattice sites are updated synchronously according to a specified rule. This rule is typically deterministic and described by Boolean algebra, but probabilistic cellular automata, for which the rules are stochastic, can also be considered. The rule is generally local in space and time, i.e., for any given time step, each site is only affected by a small number of neighboring sites, and only a small number of previous time steps.

It is clear from their definition that cellular automata are mainly designed for efficient simulation on digital computers, and at first sight it is not obvious why they should provide useful models for physical systems. However, many 'traditional' models are already very similar to cellular automata. A simple example is the Ising model, which, since its introduction in 1925 [45], has been one of the most-studied models for many body phenomena, with over 500 research papers involving

the Ising model published in 1991 alone. The Ising model and its generalization, the Potts model [46], already satisfy most of the criteria for cellular automata, except that the original models were purely static. Dynamic generalizations of the Ising model typically involve continuous time, rather than discrete time [47, 48]. However, there are many direct relations between Ising models and cellular automata. For example, Creutz [49] has shown that it is possible to construct purely deterministic cellular automata whose dynamics generate the same distribution as equivalent static Ising models. These deterministic cellular automata allow much faster computer simulations of Ising models than more conventional Monte Carlo algorithms [50]. It is also well known that cellular automata models in d spatial dimensions can be mapped to Ising models in $(d+1)$ dimensions [51].

The close connection between Ising models and cellular automata is perhaps not too surprising. More interesting is the observation by Frisch, Hasslacher, and Pomeau [52] that it is possible to construct cellular automata which, in the limit of large system size, can simulate the Navier-Stokes equation. This result is not trivial, since it is not immediately obvious how to incorporate the correct conservation laws and symmetries, like Galilean invariance, into a cellular automaton. The massively parallel algorithms available for cellular automata might therefore provide the computational capability necessary to simulate fluid flow at high Reynolds number. A potential disadvantage of cellular automata is that coarse graining over many lattice sites may be necessary to obtain a physically relevant picture [53].

Another advantage of cellular automaton models is that they allow simulations of collective behavior in large spatial dimensions. This allows numerical verification of predictions that above a certain critical dimension many body systems display trivial 'mean-field' behavior. Evidence for nontrivial collective behavior of cellular automata in five spatial dimensions has been presented in [54], where it is argued that this behavior may require new theoretical tools for its description. However, only numerical evidence is available at this time, and the argument must be regarded

as somewhat speculative.

Finally, the study of cellular automata for their own sake can be very instructive. The behavior of any given cellular automaton can be classified roughly into four categories [44]. The first category corresponds to evolution to a spatially homogeneous state, analogous to a fixed point in dynamical systems. The second category evolves to spatially periodic patterns, analogous to limit cycles in dynamical systems. The third class shows chaotic evolution, characterized by positive Lyapunov exponents [55]. The fourth class is the most complicated – cellular automata in this class are capable of *universal computation.* A computationally universal system is one that can be programmed, through its initial conditions, to simulate any digital computation. Computational universality has also been demonstrated for classical mechanical systems consisting of a set of billiard balls [56]. Computationally universal systems are necessarily nonergodic [57], since the indefinite future depends in an arbitrarily programmable way on the initial conditions. Computational universality is of course only possible in an infinite system: spatially finite systems can only evaluate 'spatially-bounded' functions [58]. We therefore expect computationally universal systems not to show scale invariance in general, since arbitrarily complex functions may become computable as the system size increases.

Although all computationally universal systems are identical in their capabilities, there may still be considerable qualitative differences between them if regarded as dynamical systems [59]. For example, suppose we have a two-dimensional computationally universal cellular automaton with two possible states per site, one or zero. It may happen that nontrivial computations only result from initial configurations where every other site has value zero, in checkerboard fashion. For random initial conditions, these configurations occur with probability zero, so that this particular automaton cannot serve as a model for 'self-organization' in nature.

The *Game of Life* [7] is a two-dimensional cellular automaton with two states per site that has been shown to be computationally universal [60]. The proof was

accomplished by explicitly constructing 'wires' out of structures which propagate without dissipation, and 'logical gates' that can perform the Boolean NAND operation [60] (see also the discussion of Boolean algebra in the Appendix). The Game of Life is therefore an extremely complex system, and computer simulations on finite lattices may not provide results that have statistical significance for large systems. Nevertheless, using arguments based on computer simulations on square lattices up to size 100×100, Bak et al. [8] maintain that the Game of Life naturally evolves to a self-organized critical state, characterized by power laws in various distribution functions. We will discuss the Game of Life in more detail in sections 2.4.2 and 2.4.3, where we present numerical evidence that the Game of Life is not critical.

2.4.2 Rules of the Game

The rules of the Game of Life are deceptively simple. The dynamics takes place on a square lattice, where each site can be either 'dead' or 'alive'. At each time step, every site is only affected by its eight nearest and next nearest neighbors. In particular

- A live site will stay alive if it has two or three live neighbors.
- A dead site will become alive if it has exactly three live neighbors.

The Game of Life can thus be considered as a simple model for a biological system, where excessive births are counterbalanced by deaths through overcrowding, and very small populations cannot survive.

The Game of Life has been one of the most popular computational pastimes, and a considerable amount of empirical data have been obtained from computer simulations [61]. When the initial density of live sites on an $N \times N$ lattice is between 0.2 and 0.7, the lattice evolves in $\sim N^2$ steps to a configuration containing a fraction of ≈ 0.03 live sites. This configuration generally consists of stable patterns, or patterns oscillating with a short temporal period. In Figure 2-8 we show a typical

section of a lattice that has reached equilibrium.

The dark circles show live sites, the hollow circles show dead sites that will become alive at the next iteration. The largest temporal period in Figure 2-8 is two. The most striking feature of Figure 2-8 is the clustering of live sites into stable configurations containing only a small number of sites, separated by relatively large distances. This is already an indication that a simple mean field theory may not be capable of predicting the asymptotic density. Possibly the simplest mean field theory consists of assigning a live probability p^n to each site at time n, and then computing the probability p^{n+1} that a site will be alive at the next time step [62]. We then obtain:

$$p^{n+1} = 28(p^n)^3(1-p^n)^5(3-p^n). \tag{2.37}$$

This equation correctly predicts a stable fixed point for $p = 0$, but it also predicts another stable fixed point for $p \approx 0.37$, which is never observed in simulations. We can improve the simple mean field theory by computing p^{n+2} from p^n. This requires the complete solution of the Game of Life in a 5×5 neighborhood, since the interaction propagates one lattice spacing in each time step. We can write p^{n+2} in the form:

$$p^{n+2} = \sum_{i=0}^{25} a_i (p^n)^i (1-p^n)^{(25-i)}, \tag{2.38}$$

where a_i is the number of configurations containing i live sites for which the central site is alive after two time steps. We show the resulting return map in Figure 2-9; the only fixed point remaining in this approximation is $p = 0$.

Higher order return maps clearly become impractical to evaluate exactly, and one needs to resort to Monte Carlo simulations to arrive at the asymptotic density of ≈ 0.03 [61].

So far we have ignored the presence of propagating structures, which are the main reasons the Game of Life can be computationally universal. By far the most common propagating structure is the *glider* (cf. Figure 2-10), which moves by one

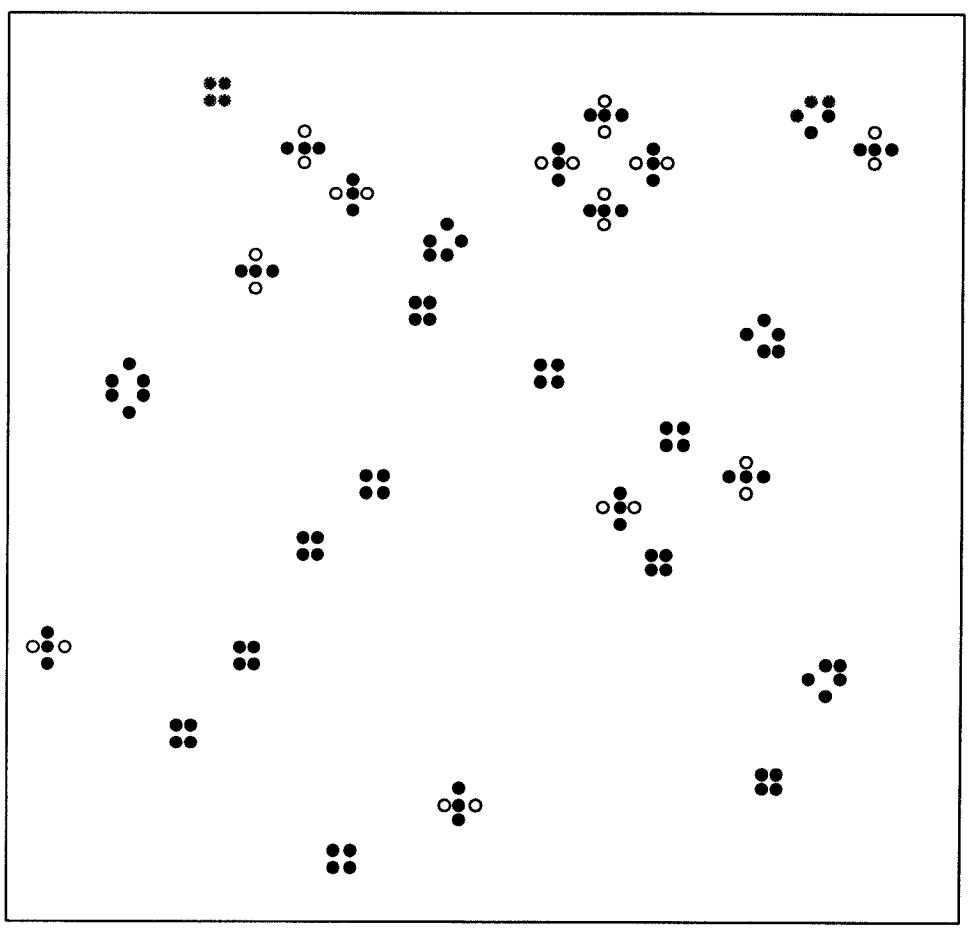

Figure 2-8: Typical Game of Life equilibrium configuration.

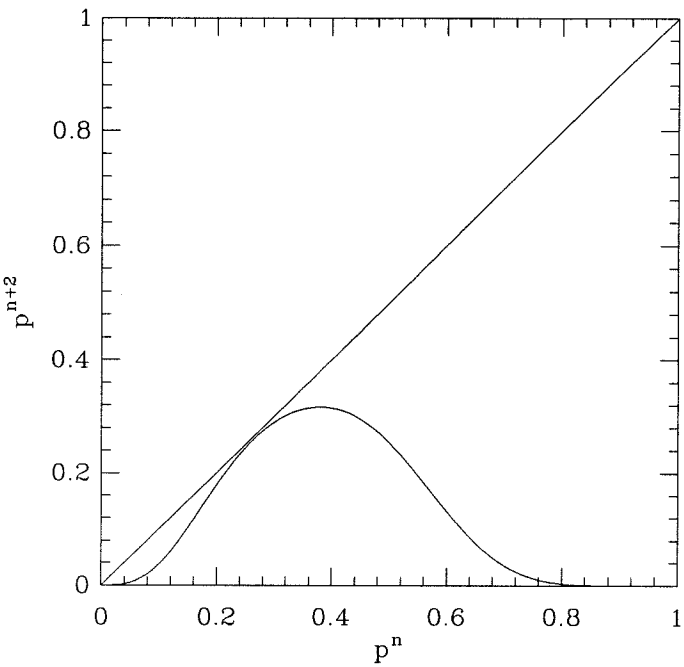

Figure 2-9: Return map for Game of Life.

diagonal square in four time steps.

Gliders are generated at a rate of approximately one per 2000 sites. Their mean free path is ≈ 25 lattice spacings [63] in a lattice that has otherwise reached equilibrium. There are particular initial configurations called *glider guns* which can continuously generate gliders [61], so that the population in an infinite system can increase indefinitely. When we speak of equilibrium in a finite lattice, we therefore mean configurations where propagating structures have either escaped to infinity,

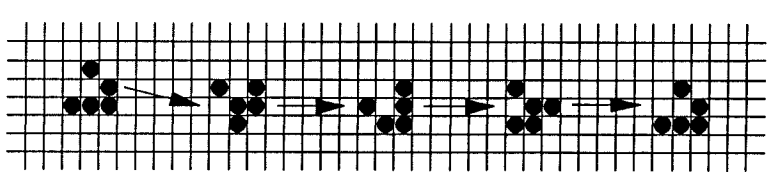

Figure 2-10: The glider.

or have been halted at the boundary.

Bak et al. [8] have presented numerical evidence that if an equilibrium Life configuration is repeatedly perturbed, the distribution of the relaxation times $D(T)$ before equilibrium is reestablished follows a power law $D(T) \sim T^{-1.6}$. This would suggest that the equilibrium configuration rearranges itself to a minimally stable state, where perturbations can propagate an arbitrary distance. In the next section, we will present numerical evidence that the distribution $D(T)$ is in fact exponential of the form $D(T) \sim \exp(-T/T_0)$, where T_0 is a characteristic time scale of an avalanche [64].

2.4.3 Numerical Simulations

In any numerical investigation of scaling behavior it is important to be aware of the relevant scales involved. The most obvious scales in a finite lattice are the lattice spacing on the one hand, and the lattice size L on the other hand. Identifying intermediate scales will depend on the particular system in question. From Figure 2-8 it appears that stable clusters in the Game of Life are separated by 10 or more lattice spacings, so that we may expect intermediate length scales of that order. The obvious time scale for the Game of Life is the time it takes for a random configuration to relax to equilibrium; this time is always finite in a finite system. If the *driven* system indeed displays self-organized criticality, it must do so over a time scale larger than the relaxation time of the *undriven* system.

In Figure 2-11 we show the distribution of relaxation times for two lattices size 256×256 and 512×512, starting from a random initial configuration, without external driving.

Asymptotically we find the distribution function to take the form $D(T) \sim \exp(-T/T_0)$, where $T_0 \approx 1850$ independent of the lattice size. We conclude that T_0 is an important time scale for the undriven system, and to convincingly demonstrate scaling behavior for the driven system we need to accumulate data over several

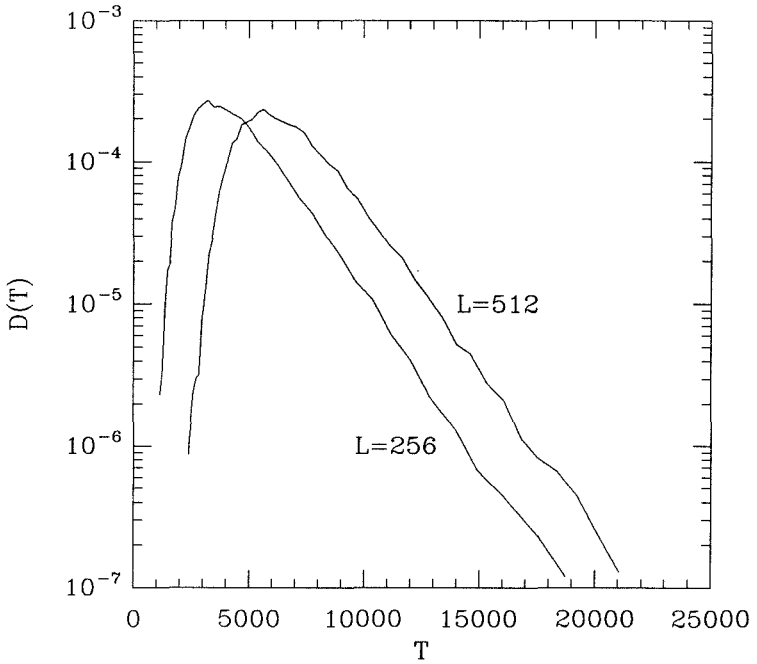

Figure 2-11: Life relaxation times, undriven system.

factors of T_0.

In Figure 2-12 we present our results for $D(T)$ for the driven system, where each relaxation time T is the result of a single perturbation to a system which has relaxed to equilibrium from a previous perturbation.

We again find an exponential distribution for large T, with the same time constant T_0 as the undriven system. The data for lattice sizes 256×256 and 512×512 are virtually identical, indicating that the finite relaxation time is indeed the result of a finite correlation length, rather than a finite size effect.

In addition to the relaxation time T_0, it is also useful to measure the correlation length L_0 to compare with the system size L. We can obtain a rough estimate of L_0 by measuring the net number A of sites that are changed during an avalanche, which should be approximately proportional to the area covered by the avalanche. In Figure 2-13 we show that A is roughly proportional to the duration T indicating

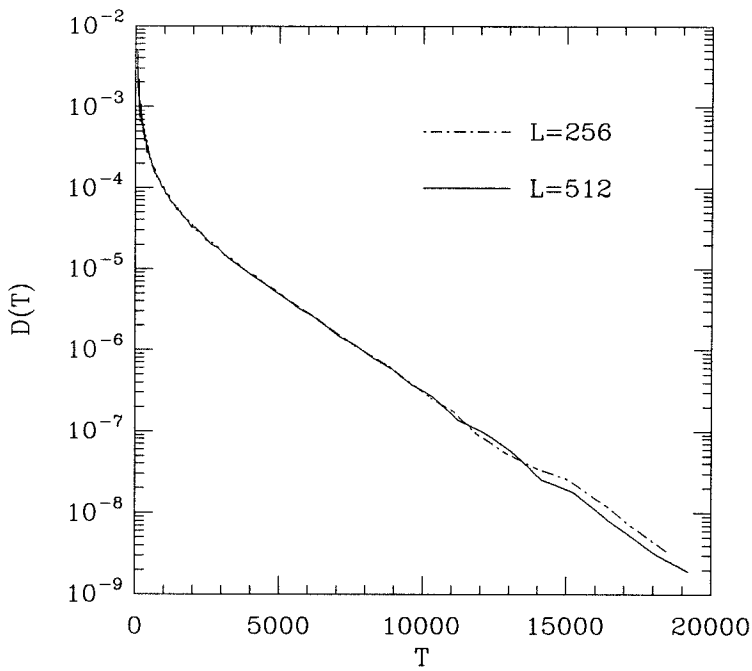

Figure 2-12: Life relaxation times, driven system.

that avalanches are propagating similar to an ordinary diffusive random walk. Note that the y-intercept is not zero because even at equilibrium there is a background activity on the lattice due to local oscillators, which we have not subtracted out.

To obtain an estimate of the actual spatial size of an avalanche, we use our knowledge that the equilibrium density is ≈ 0.03. We find that an avalanche with duration $T_0 \approx 1850$ covers an area of ≈ 8000 sites, leading to an estimate for the correlation length $L_0 \approx 50$.

To determine L_0 more precisely, we perturb the lattice not at a single point at a time, but along a whole edge, which we call a 'hot' boundary. We then measure the active and passive densities as a function of the distance away from the hot boundary (the active density is defined by live sites not alive six steps ago). We show our results in Figure 2-14, for a lattice size 256×488 with the hot boundary on the left, a closed boundary on the right, and periodic boundary conditions in the

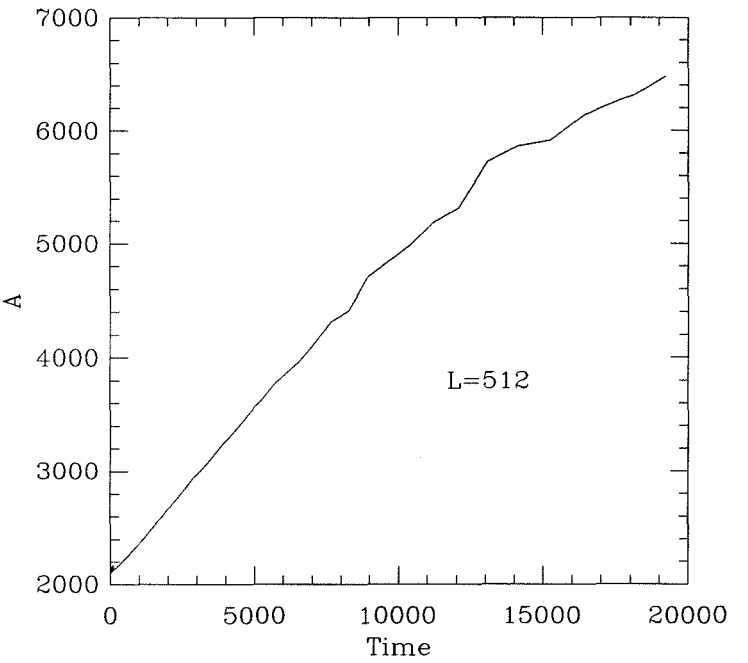

Figure 2-13: Number of sites changed during avalanche.

vertical direction.

The passive density approaches the characteristic equilibrium value ≈ 0.03 away from the hot boundary, while the active density decreases exponentially with a characteristic length $L_0 = 42 \pm 3$. We obtained equivalent results for lattices of vertical size 128, thereby verifying that our results are not affected by vertical correlations.

To summarize, we have obtained strong numerical evidence that the Game of Life is subcritical with a large but finite relaxation time $T_0 \approx 1850$, independent of whether the system relaxes to equilibrium from random initial conditions, or from repeated perturbations at isolated points. We estimate a correlation length $L_0 \approx 42 \pm 3$. This suggests that the numerical results presented by Bak et al. [8] for system size 100×100 are strongly influenced by finite size effects.

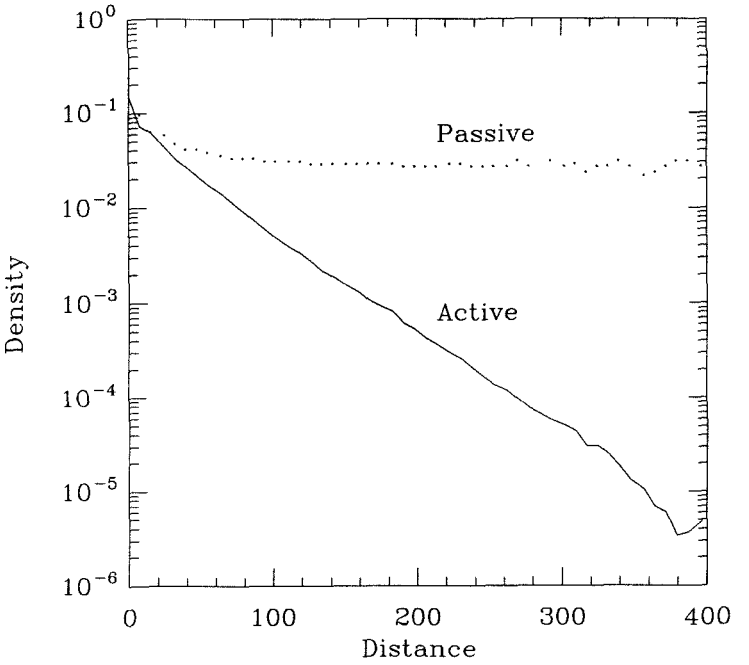

Figure 2-14: Active and passive densities away from hot boundary.

2.4.4 A Universe Model

We emphasize that the numerical results presented in section 2.4.3 do not exclude the possibility that the Game of Life may be metastable with respect to nucleation events too rare to have occurred in any computer simulation to date. However, our simulations strongly suggest that these metastable states, if they indeed exist, do not occur 'naturally' as a result of repeated driving, as required by self-organized criticality.

In this context we briefly describe another cellular automaton, called the *universe model* [65], which we believe illustrates another way one might erroneously interpret numerical simulations as showing self-organized criticality. In contrast with the Game of Life, the universe model does not display a definite correlation length independent of the system size. Instead, the distribution of relaxation times decays exponentially with a time constant that increases with system size. At first sight

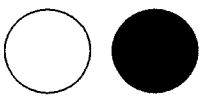

Figure 2-15: Glider in universe model.

this suggests that the model is indeed critical, since the system size is the only relevant length scale. However, we will argue that in this case the relaxation times result from relaxations of states which are only stabilized by finite size effects. Such states do not occur in the infinite size limit, and it is therefore meaningless to talk about critical fluctuations around these states.

The universe model is defined on any d-dimensional hypercubic lattice, with three possible states per site, 'active', 'passive', and 'empty'. The rules are:

1. Active sites at time t 'burn out' and become passive at time $t + 1$.

2. Passive sites are annihilated and become empty when they have exactly one active neighbor.

3. Empty sites become active when the have exactly one active neighbor which has a passive site at the opposite position.

Rule 3 allows the existence of 'gliders' as in the Game of Life. The configuration shown in Figure 2-15 propagates to the right with unit velocity, where the filled circle represents an active site, while the empty circle represents a passive site (in the figure, all other neighbors are empty sites).

In their simulations, Chen et al. [65] start with a random initial distribution of active, passive, and empty sites and let the system come to rest with no active sites remaining. As in the Game of Life, the system is then repeatedly perturbed by adding a single propagating particle, and the relaxation times to return to rest are measured. As this process is repeated, the system is believed to evolve to a statistically stationary state, with power law distributions in the relaxation times [65].

In our simulations, we *continually* start with a random initial configuration, rather than repeatedly perturb one that has come to rest. We find that the distribution $D(T)$ of relaxation times has the form $D(T) \sim T\exp(-T/T_0)$, where T_0 increases rapidly with system size. In Figures 2-16a and 2-16b we show $D(T)$ for system sizes 60×60 and 92×92. In Figure 2-16c we plot the relaxation time T_0 for system sizes ranging from 28×28 to 156×156.

Figure 2-16c shows that T_0 increases approximately exponentially with system size. This result suggests that configurations with no active sites will have negligible probability in the large system limit. By extensive simulations on a system of size 384×384 we estimate that the steady state density of active sites is ≈ 0.0088.

To summarize, we have shown that finite size effects are probably responsible for the apparent scale invariance observed in two cellular automaton models. In this context we mention that numerical evidence has been presented [66] that yet another cellular automaton, called the 'forest fire' model, does not seem to show nontrivial scaling behavior as had previously been suggested [67].

2.5 Conclusion

Our investigations of self-organized criticality have included two broad classes of models. The first class contains the sandpile models, for which we have presented a simple mean field theory which predicts power law behavior under very general conditions. The second class contains cellular automata which can be considered as crude models of biological systems. We have presented numerical evidence that the scale invariance reported for two such models was due to finite size effects and does not appear to hold for larger systems.

We have also presented a third scenario under which nontrivial scaling behavior can occur, by studying a variant of the Barenblatt equation. The scaling behavior is particularly complicated because the scaling exponent depends continuously on a

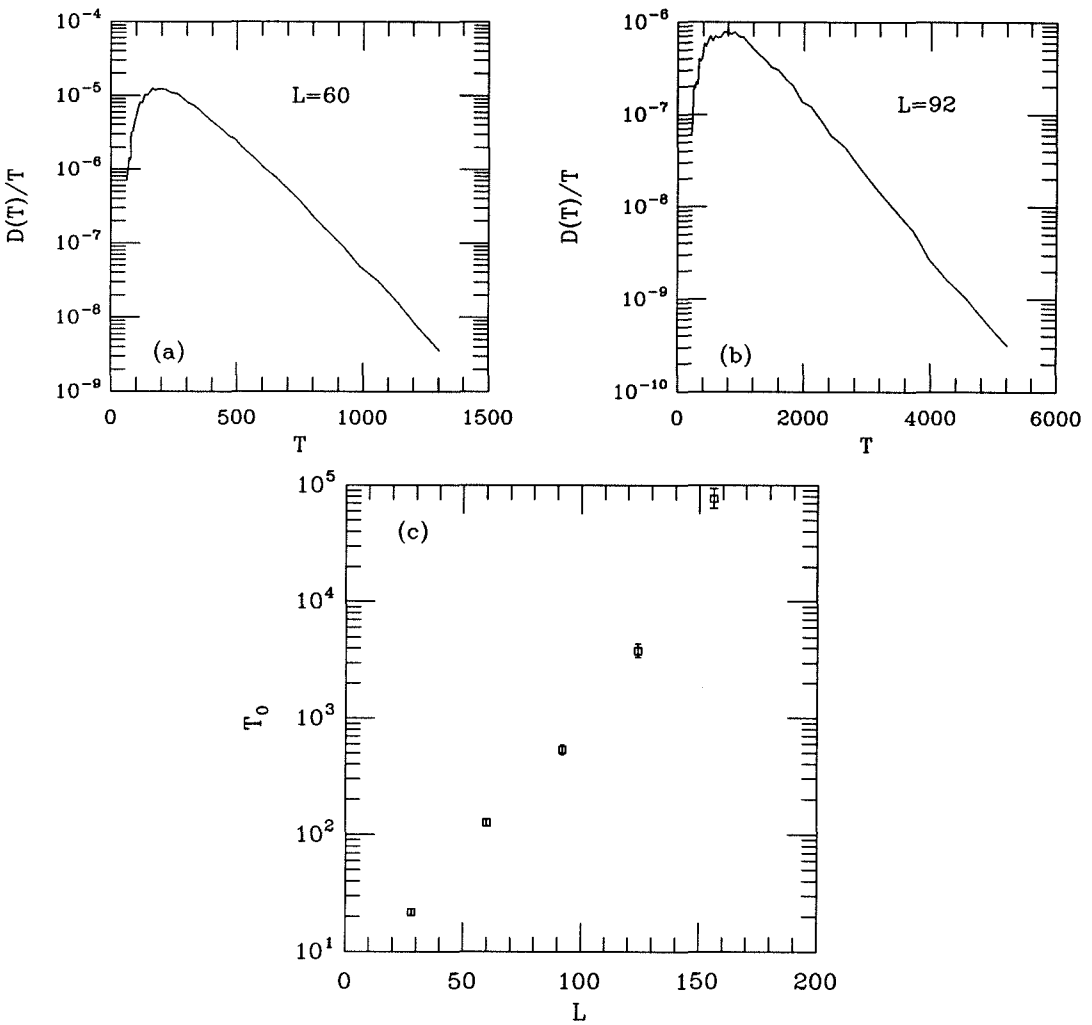

Figure 2-16: Universe model (a) $D(T)$ for $L = 60$ (b) $D(T)$ for $L = 92$ (c) T_0 versus L.

parameter in the model. This scenario does not seem to apply to any of the models studied under self-organized criticality.

Appendix

In this Appendix we briefly review the basics of Boolean algebra as it applies to the numerical simulation of cellular automata.

Boolean algebra consists of binary operations carried out on binary values which can be either 0 or 1. For example, the result of the operation A AND B gives 1 if and only if both A and B are 1. Similarly, the operation A OR B gives 1 if either A or B is 1. Another important operation is the XOR operation. A XOR B gives 1 if either A or B is 1, but not both. Finally, the unary operation NOT reverses the value of its operand, e.g., NOT 0 gives 1.

Any dynamical rule that can be stated as an operation involving Boolean algebra can be efficiently implemented on digital computers since they typically carry out several Boolean operations in parallel. This has been utilized in simulations of the Ising model [50], where large lattices sizes can be simulated with the help of this parallelization.

Here we describe how the Game of Life can be formulated in terms of Boolean algebra. We first need a way to represent the number of live neighbors n of a given lattice site c. Since n can range from zero to eight, and a Boolean variable can only take on two values, we write n in binary notation as

$$n = b_3 \times 8 + b_2 \times 4 + b_1 \times 2 + b_0 \times 1, \tag{2.39}$$

where $b_0, \ldots, b_3$ are all Boolean variables. If we treat c as a Boolean variable taking on the value 0 if the cell is dead and the value 1 if the cell is alive, the rules of the

Game of Life (cf. section 2.4.2) can be implemented as:

$$c = (c\ OR\ b_0)\ AND\ b_1\ AND\ (NOT\ b_2)\ AND\ (NOT\ b_3), \qquad (2.40)$$

where c will have the correct value after the logical operations. We also need to implement the process of addition as a set of Boolean operations. This can be accomplished by observing that if we are given two Boolean variables t_1 and t_2, we can add them in binary notation by the operations $b_1 = t_1\ AND\ t_2$, and $b_0 = t_1\ XOR\ t_2$. Using this procedure, we can add the values of the eight neighbors to arrive at Eq. (2.39).

In principle, we could use a similar procedure to simulate the sandpile models of section 2.3.3. However, since in this case the actual number of sites toppling at any given time is usually much smaller than the number of lattice sites, it is more efficient to simply update a list of the sites that need to be toppled.

References

[1] See, e.g., H.E. Stanley, *Introduction to Phase Transitions and Critical Phenomena* (Oxford University Press 1971).

[2] See, e.g., K.G. Wilson, Rev. Mod. Phys. **47**, 773 (1975).

[3] See, e.g., S.K. Ma, *Modern Theory of Critical Phenomena* (Benjamin Publishing Company 1976).

[4] For reviews of 1/f noise, see P. Dutta and P.M Horn, Rev. Mod. Phys. **53**, 497(1981); M.B. Weissman, Rev. Mod. Phys. **60**, 537(1988).

[5] P. Bak, C. Tang, and K. Wiesenfeld, Phys. Rev. Lett. **59**, 381 (1987) and Phys. Rev. **A38**, 364 (1988).

[6] G.I. Barenblatt, *Similarity, Self-Similarity, and Intermediate Asymptotics*, Consultants Bureau, New York, (1979).

[7] J.H. Conway, unpublished (1970).

[8] P. Bak, K. Chen, and M. Creutz, Nature **342**, 780 (1989).

[9] P.W. Bridgeman, *Dimensional Analysis*, Yale University Press (1931).

[10] E. Buckingham, Phys. Rev. **14**, 345 (1914).

[11] G.I. Taylor, Proc. Roy. Soc. **201**, 175 (1950).

[12] J.M. Carlson, J.T. Chayes, E.R. Grannan, and G.H. Swindle, Phys. Rev. **A42**, 2467 (1990).

[13] L.P. Kadanoff, S.R. Nagel, L. Wu, and S. Zhou, Phys. Rev. **A39**, 6524 (1988).

[14] T.C. Halsey, M.H. Jensen, L.P. Kadanoff, I. Procaccia, and B.I. Shraiman, Phys. Rev. **A33**, 1141 (1986).

[15] S.L. Kamenomostskaya, Dokl. Akad. Nauk SSSR **116**, 18 (1957).

[16] L.P. Kadanoff, A.B. Chhabra, A.J. Kolan, M.J. Feigenbaum, and I. Procaccia, Phys. Rev. **A45**, 6095 (1992).

[17] N. Goldenfeld, O. Martin, Y. Oono, and F. Liu, Phys. Rev. Lett. **64**, 1361 (1990).

[18] *Handbook of Mathematical Functions*, M. Abramowitz and I. Stegun eds., Dover Publications 1970.

[19] B. Grossmann, H. Guo, and M.Grant, Phys. Rev. **A41**, 4195 (1990); P. Grassberger and S. S. Manna, J. Phys. **51**, 1077 (1990).

[20] S. S. Manna, J. Stat. Phys. **59**, 509 (1990).

[21] J.M. Carlson, J.T. Chayes, E.R. Grannan, and G.H. Swindle, Phys. Rev. Lett. **65**, 2547 (1990).

[22] D. Dhar, Phys. Rev. Lett. **64**, 1613 (1990).

[23] S. S. Manna, Physica A **179**, 249 (1991).

[24] P. Evesque, Phys. Rev. **A43**, 2720 (1991).

[25] H.M. Jaeger, C.H. Liu, and S.R. Nagel, Phys. Rev. Lett. **62**, 40 (1989).

[26] G.A. Held, D.H. Solina, D.T. Keane, W.J. Haag, P.M. Horn, and G. Grinstein, Phys. Rev. Lett. **65**, 1120 (1990);

[27] T. Hwa and M. Kardar, Phys. Rev. Lett. **62**, 1813 (1989).

[28] A. Diaz-Guilera, Phys. Rev. **A45**, 8551 (1992).

[29] G. Grinstein and D.-H. Lee, Phys. Rev. Lett. **66**, 177 (1991).

[30] G. Grinstein, D.-H. Lee, and S. Sachdev, Phys. Rev. Lett. **64**, 1927 (1990).

[31] D. Forster, D.R. Nelson, and M.J. Stephen, Phys. Rev. **A16**, 732 (1977).

[32] D. Dhar and R. Ramaswamy, Phys. Rev. Lett. **63**, 2659 (1989).

[33] T. Hwa and M. Kardar, Phys. Rev. **A45**, 7002 (1992).

[34] C. Tang and P. Bak, J. Stat. Phys. **51**, 797 (1988).

[35] J. Theiler, unpublished.

[36] T. E. Harris, *The Theory of Branching Processes*, Springer-Verlag (1963).

[37] H. W. Watson and F. Galton, J. Anthropol. Inst. Great Britain and Ireland **4**, 138 (1874).

[38] R. Otter, Annals of Math. Stat. **20**, 206 (1949).

[39] As quoted in ref [36], p.21.

[40] D. Dhar and S. N. Mayundar, J. Phys. A **23**, 4333 (1990).

[41] C. H. Bennett and M. S. Bourzutschky, unpublished; H. J. S. Feder and J. Feder, Phys. Rev. Lett. **66**, 2669 (1991).

[42] K. Christensen, H. C. Fogedby, and H. J. Jensen, J. Stat. Phys. **63**, 718 (1991).

[43] J. von Neumann, *Collected Works* **5**, 288 (1961).

[44] For a general review of cellular automata, see S. Wolfram, Rev. Mod. Phys. **55**, 601 (1983).

[45] E. Ising, Z. Phys. **31**, 253 (1925).

[46] For a review of the Potts model, see F. Y. Wu, Rev. Mod. Phys. **54**, 235 (1982).

[47] R. J. Glauber, J. Math. Phys. **4**, 294 (1963).

[48] K. Kawasaki, Phys. Rev. **150**, 285 (1966).

[49] M. Creutz, Phys. Rev. Lett. **50**, 1411 (1983), J. Stat. Phys. **42**, 823 (1986).

[50] B. Hede and H. J. Herrmann, J. Phys. A **24**, L691 (1991).

[51] A. M. A. Verhagen, J. Stat. Phys. **15**, 213 (1976); E. Domany and W. Kinzel, Phys. Rev. Lett **53**, 311 (1984).

[52] U. Frisch, B. Hasslacher, and Y. Pomeau, Phys. Rev. Lett. **56**, 1505 (1986).

[53] S. Wolfram, J. Stat. Phys. **45**, 471 (1986).

[54] H. Chaté and P. Manneville, Europhys. Lett. **14**, 409 (1991).

[55] N. Packard and S. Wolfram, J. Stat. Phys. **38**, 901 (1985).

[56] E. Fredkin and T. Toffoli, Int. J. Theor. Phys. **21**, 219 (1982).

[57] C. H. Bennett and G. Grinstein, Phys. Rev. Lett. **55**, 657 (1985).

[58] S. Wolfram, Physica D **10**, 1 (1984).

[59] S. Wolfram, Physica Scripta T **9**, 170 (1985).

[60] E. R. Berlekamp, J. H. Conway, and R.K. Guy, *Winning Ways for Your Mathematical Games*, Vol. 2, Academic Press (1982).

[61] M. Gardner, *Mathematical Games*, Sci. Amer. **224**, Feb. 112 (1971), and *Wheels, Life and Other Mathematical Amusements*, W. H Freeman (1983).

[62] L. S. Schulman and P. E. Seiden, J. Stat. Phys. **19**, 293 (1978).

[63] C. H. Bennett, private communication.

[64] C. H. Bennett and M. S. Bourzutschky, Nature **350**, 468 (1991).

[65] K. Chen and P. Bak, Phys. Lett. A **140**, 299 (1989).

[66] P. Grassberger and H. Kantz, J. Stat. Phys. **63**, 685 (1991).

[67] P. Bak, K. Chen, and C. Tang, Phys. Lett. **A**147, 297 (1990).